B- AND A-TYPE STARS IN THE TAURUS–AURIGA STAR-FORMING REGION

KUNAL MOOLEY[1], LYNNE HILLENBRAND[1], LUISA REBULL[2], DEBORAH PADGETT[2,4], AND GILLIAN KNAPP[3]

[1] Department of Astronomy, California Institute of Technology, 1200 East California Boulevard, MC 249-17, Pasadena, CA 91125, USA; kunal@astro.caltech.edu
[2] Spitzer Science Center, California Institute of Technology, Pasadena, CA 91125, USA
[3] Department of Astrophysics, Princeton University, Princeton, NJ 08544, USA

ABSTRACT

We describe the results of a search for early-type stars associated with the Taurus–Auriga molecular cloud complex, a diffuse nearby star-forming region noted as lacking young stars of intermediate and high mass. We investigate several sets of possible O, B, and early A spectral class members. The first is a group of stars for which mid-infrared images show bright nebulae, all of which can be associated with stars of spectral-type B. The second group consists of early-type stars compiled from (1) literature listings in SIMBAD, (2) B stars with infrared excesses selected from the *Spitzer Space Telescope* survey of the Taurus cloud, (3) magnitude- and color-selected point sources from the Two Micron All Sky Survey, and (4) spectroscopically identified early-type stars from the Sloan Digital Sky Survey coverage of the Taurus region. We evaluated stars for membership in the Taurus–Auriga star formation region based on criteria involving: spectroscopic and parallactic distances, proper motions and radial velocities, and infrared excesses or line emission indicative of stellar youth. For selected objects, we also model the scattered and emitted radiation from reflection nebulosity and compare the results with the observed spectral energy distributions to further test the plausibility of physical association of the B stars with the Taurus cloud. This investigation newly identifies as probable Taurus members three B-type stars: HR 1445 (HD 28929), τ Tau (HD 29763), 72 Tau (HD 28149), and two A-type stars: HD 31305 and HD 26212, thus doubling the number of stars A5 or earlier associated with the Taurus clouds. Several additional early-type sources including HD 29659 and HD 283815 meet some, but not all, of the membership criteria and therefore are plausible, though not secure, members.

Key words: ISM: clouds – stars: early-type – stars: formation – stars: variables: T Tauri, Herbig Ae/Be

Online-only material: color figures, machine-readable table

1. INTRODUCTION

The Taurus–Auriga molecular cloud complex (hereafter "Taurus") is the quintessential region of nearby recent star formation. It is characterized by low star formation efficiency (Goldsmith et al. 2008) and the absence of high-mass young stars (Kenyon et al. 2008) and stands in contrast to more distant, massive, and dense star-forming environments like the Orion molecular clouds. Taurus lies at a mean distance of about 140 pc with a depth of 20 pc or more (Kenyon et al. 1994; Torres et al. 2007, 2012) and spans approximately 100 deg^2 on the sky, or about a 25 pc diameter at this distance. The few times 10^4 $M_\odot$ cloud currently has over 350 known members, mainly sub-stellar and low-mass stellar objects with $M < 0.5$ $M_\odot$, and only about 10 members identified with $M > 1.5$ $M_\odot$. Much effort over the past decade in Taurus has been directed toward completely defining the low-mass stellar and sub-stellar population.

A comprehensive review of Taurus is given by Kenyon et al. (2008). Major recent contributions to our knowledge include: (1) mapping of the molecular gas (Goldsmith et al. 2008; Narayanan et al. 2008) and dust (Lombardi et al. 2010; Palmeirim et al. 2013) comprising the cloud, (2) determination of the distance of individual young star members through very long baseline interferometry (VLBI; Torres et al. 2009) parallaxes, (3) improvement of the young stellar object (YSO) census including new stellar and brown dwarf candidate members (Rebull et al. 2010, 2011; Luhman et al. 2009, 2010; Takita et al. 2010) as well as new companions to already known objects (Kraus et al. 2011), (4) measurement of proper motions using optical and VLBI techniques (Torres et al. 2009; Luhman et al. 2009), (5) provision of evidence for mass segregation (Kirk

& Myers 2011; Parker et al. 2011), and (6) searches for outflows (Narayanan et al. 2012; Bally et al. 2012).

In particular, a *Spitzer* program directed at Taurus (Güdel et al. 2007; PI: D. Padgett) produced large-scale multiwavelength maps of the clouds. Photometry from this survey has improved our understanding of both the stellar/sub-stellar membership and the incidence of protoplanetary disks (Rebull et al. 2010). Motivating the investigation described in this paper are four large and two smaller reflected and/or scattered-light nebulae found in these mid- and far-infrared (IR) images, shown in Figure 1.

Each of the large IR nebulae is illuminated by a point source that is a known B or A0 star. Two of these, HD 28149 (72 Tau) and HD 29647, have been studied in the literature to date (e.g., Kenyon et al. 1994; Whittet et al. 2001, 2004) as background stars and used to derive the physical and chemical properties of the molecular cloud. One source, HD 282276, was unstudied until noted by Rebull et al. (2010, 2011) to have a mid-IR excess. Finally, V892 Tau is a well-known Herbig Ae/Be type member of Taurus (Elias 1978) that also illuminates an optical reflection nebula—an original defining characteristic of the Herbig Ae/Be population. The two additional smaller IR nebulae are likewise associated with early-type or high-luminosity stars. HD 28929 = HR 1445 has been known as a chemically peculiar star (e.g., Wolff & Preston 1978) but has not otherwise distinguished itself in the literature. IC 2087 is associated with a known YSO (Elias 1978) and, like V892 Tau, illuminates an optical nebula. The nebular regions for all six of these sources appear brightest at mid-IR wavelengths; optical nebulosity is generally absent, but when apparent, is weaker, except in the case of IC 2087.

The proximity of these early-type stars to cloud material, as evidenced by the mid-IR nebulae, suggests that rather than being background stars as they have traditionally been considered,

---

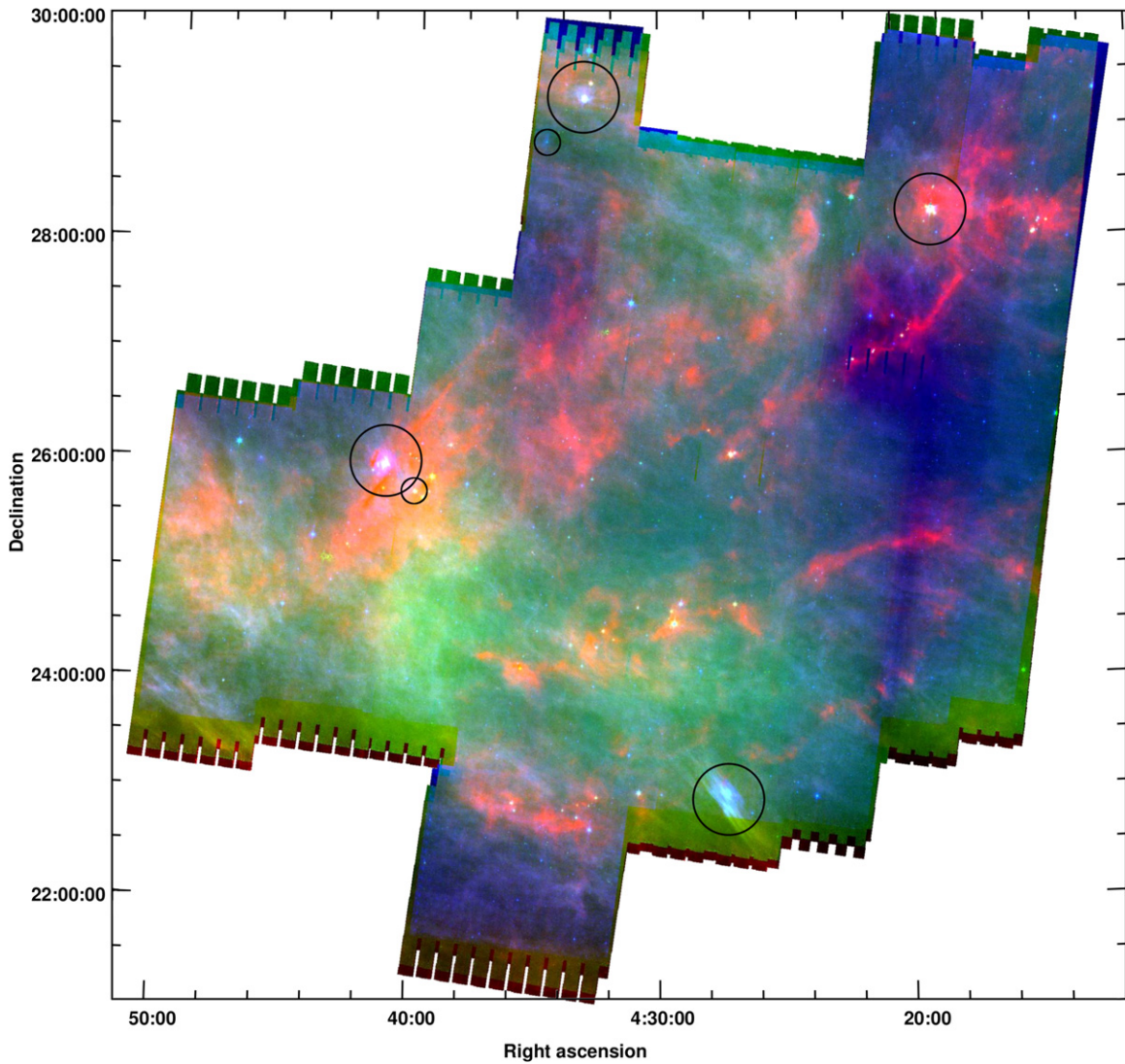[4] Current address: Goddard Space Flight Center, Greenbelt, MD, USA.

Figure 1. *Spitzer* mosaic of IRAC and MIPS images of Taurus. Color coding: 8 (blue), 24 (green), and 160 (red) μm. Four bright and large nebulous objects illuminated by B stars are evident in this mosaic. They have been marked with large circles and are associated with: (1) top middle: HD 282276, (2) top right: V892 Tau (Elias 1), (3) bottom middle: HD 28149 (72 Tau), and (4) middle left: HD 29647. Two fainter and weaker nebulae are marked with smaller circles and are associated with: (5) top middle: HD 28929 (HR 1445), (6) middle left: IC 2087.

(A color version of this figure is available in the online journal.)

they may be heretofore unappreciated early-type members of Taurus. The association of these stars with prominent nebulosity is not, however, sufficient evidence that they are genuine members of Taurus. Instead, they could be stars of early type that are physically unassociated but fortuitously located with respect to either the Taurus molecular cloud complex itself or smaller patches of locally enhanced density in the foreground or background interstellar medium (ISM). Reminiscent of this latter situation is the Pleiades star cluster, which is passing through and illuminating denser-than-average ISM that is physically unassociated with the stars themselves. In this contribution, we explore the evidence and attempt to distinguish between these two scenarios.

The earliest-type Taurus members are generally considered (Kenyon et al. 2008; Rebull et al. 2010) to be IC 2087-IR (estimated at B5 based on bolometric luminosity but a heavily self-embedded star with a continuum-emission optical spectrum), the binary system V892 Tau (Elias 1; a B8-A6 self-embedded Herbig Ae/Be star with a near-equal brightness companion), the triple system HD 28867 (B8+2×B9.5), AB Aur

(A0e, a Herbig Ae/Be star), and HD 31648 (MWC 480; A2e, another Herbig Ae/Be star). There are no associated F stars[5] and the next earliest types are HP Tau/G2 (G0) and SU Aur (G2). Notably, almost all of these earliest-type members of Taurus harbor significant amounts of circumstellar material, with the HD 28867 system[6] being the exception.

While no systematic investigation for high-mass stars associated with Taurus has been performed recently, there has been historical interest in early-type stars seen toward this canonically low-mass star-forming region. Blaauw (1956) identified Casseiopeia-Taurus (hereafter Cas-Tau) as an OB association lying between 140 and 220 pc using the convergent-point method. A debate ensued concerning the relationship of the young Taurus–Auriga molecular cloud to the older

---

[5] HD 283759 (F2–F3) and V410-Anon24 (F9–G3) have at various times been suggested as members, but both are well underluminous with respect to the other stars in this list if assumed to be at the same distance, and not particularly obscured.

[6] This source is to the south of the main Taurus–Auriga clouds, in the L 1551 region, and is not otherwise discussed in this paper; see Walter et al. (2003).

Table 1
Number of O, B Stars Known to SIMBAD toward Taurus (Central Rectangle)
and Neighboring Regions of Equivalent Area in Coordinates of
Galactic Latitude and Galactic Longitude

	195°	180°	165°	150°
0°				
	304	513	342	
-10°				
	100	117	122	
-20°				
	32	46	33	
-30°				

Cas-Tau OB association, but it has now been resolved that they are unrelated in both space and age (see below). The first early-type stars associated with the Taurus clouds was AB Aur, an original Ae/Be star associated with optical nebulosity (Herbig 1960), followed by the IR-selected YSOs V892 Tau and IC 2087-IR (Elias 1978).

How many higher-mass stars should there be in Taurus? Using the number and distribution of the known low-mass T Tauri stars and the assumption that weak-lined T Tauri stars are far more numerous (as high as 10:1) than classical T Tauri stars, Walter et al. (1988) argued from a sparse X-ray survey of Taurus with *Einstein* that there should be $\sim 10^3$ low-mass members of Taurus. The initial mass function (IMF) appropriate for young star clusters (Miller & Scalo 1979) would then predict the existence of tens of B-type members. The search for these B stars culminated with Walter & Boyd (1991) identifying 29 possible members of the Taurus–Auriga T association based on spectroscopic parallax and proper motion. However, the large number of low-mass Taurus member stars predicted by Walter et al. (1988) were not found in the proper-motion survey by Hartmann et al. (1991), who suggested that many of the stars found in the X-ray survey by Walter et al. (1988) belong to the older and more distant Cas-Tau group, and that the assumption of a uniform distribution of T Tauri stars is not correct. While Walter & Boyd (1991) had concluded that the Tau-Aur T association was related to the Cas-Tau OB association, de Zeeuw et al. (1999) showed that these are kinematically distinct groups and rejected the Walter & Boyd (1991) stars as Cas-Tau members.

Most subsequent publications on the Taurus–Auriga stellar population have focused on the low-mass stars. However, of relevance to the present study is that Whittet et al. (2004) proposed, on the basis of extinction and dust modeling, that HD 29647 (B9III) is located within a diffuse screen surrounding the dense molecular clump TMC-1 in Taurus. Also, Rebull et al. (2010) suggested that its IR excess and spectroscopic parallax make HD 27659 (A0–A4V) a high-quality candidate member of Taurus, and that HD 282276 (B8V) and HD 283815 (A0V) are lower-quality, but plausible, candidate members. As the situation concerning associated early-type stars remains unclear, and considering the high level of interest in the membership and star formation history of Taurus, a detailed investigation using the wealth of new information seems warranted.

This paper is organized as follows. In Section 2, we describe the process of compiling the list of early-type stars toward Taurus (Section 2.2) and testing these stars for membership (Section 2.3). Our literature survey showed that spectral typing and age estimation of some of the early-type stars were done decades ago with prism-based spectrometers, and so we considered the possibility that some have been assigned an incorrect spectral type. Additionally, we considered that some early-type stars could have been missed due to limits on the spatial extent or photometric depth of previous investigations. We spectroscopically followed up all probable members (Section 2.4). Given our initial motivation for this investigation, reflection/scattered-light nebulae toward several known B stars, we then describe the modeling procedure for the scattered/thermal dust emission in Section 2.5. Detailed discussion of our findings and results for individual objects are provided in Section 3. We conclude with a summary and discussion in Section 4.

2. DATA COLLECTION AND ANALYSIS

2.1. Overview

Working from the evidence of early-type members provided by the reflection/scattered-light nebulae and the recent suggestions of additional B- and A0-type stars as plausible members, we carried out a new search for stars of spectral classes O–A0 associated with Taurus. The areal extent of our study is the region bounded by 4^h and 5^h in right ascension and $22°$ and $31°$ in declination. In galactic coordinates, this is roughly the region $(165, -20) \lesssim (l, b) \lesssim (180, -10)$. This boundary was chosen to include most of the dense cores in Taurus but not to be so large as to obfuscate the search with unassociated early-type stars at different distances. The region south of the Taurus main cloud between 4^h3 and 4^h9 in right ascension and $16°$ and $20°$ in declination is also considered a part of the Taurus star-forming region, but is not included in this investigation.

We first looked at whether there is a concentration of early-type stars toward or away from the large patch of sky under consideration. A SIMBAD query for known O, B stars toward Taurus and eight neighboring regions of equal areal extent results in the distribution shown in Table 1. There is a higher density of known early-type stars in the direction of the galactic plane as expected, and no particular bias of early-type stars at the longitude of Taurus compared to adjacent longitudes. Thus, from our study, we expect to find only a few known early-type stars, if any, that are genuinely associated with Taurus.

In order to compile the list of candidate early-type stars toward Taurus, we gathered multiwavelength photometric and spectroscopic data and images, and collected information from the literature. We then passed these stars through two membership tests: appropriate distance and appropriate kinematics. All candidates satisfying these two criteria were labeled as probable members of Taurus. These likely members, along with other stars meeting some but not all of the criteria, were followed up spectroscopically.

2.2. Compiling the List of Candidate Early-type Stars and Ancillary Data

Four data sets were used to assemble a list of early-type stars toward the Taurus region: (1) previously identified O- and B-type stars listed in SIMBAD, (2) proposed B and early A stars with IR excesses selected from the *Spitzer* survey of the Taurus cloud discussed in Rebull et al. (2010), (3) photometrically selected point sources from the Two Micron All Sky Survey Point Source Catalog (2MASS-PSC; Skrutskie et al. 2006), and (4) spectroscopically identified early-type stars from the Sloan Digital Sky Survey (SDSS) observations of the Taurus region (Finkbeiner et al. 2004) presented by Knapp et al. (2007). As illustrated in Figure 2, there is only partial coverage of the total cloud region (see also Figure 4) in each of SDSS and the Rebull et al. (2010) *Spitzer* surveys, and the overlap between the optical
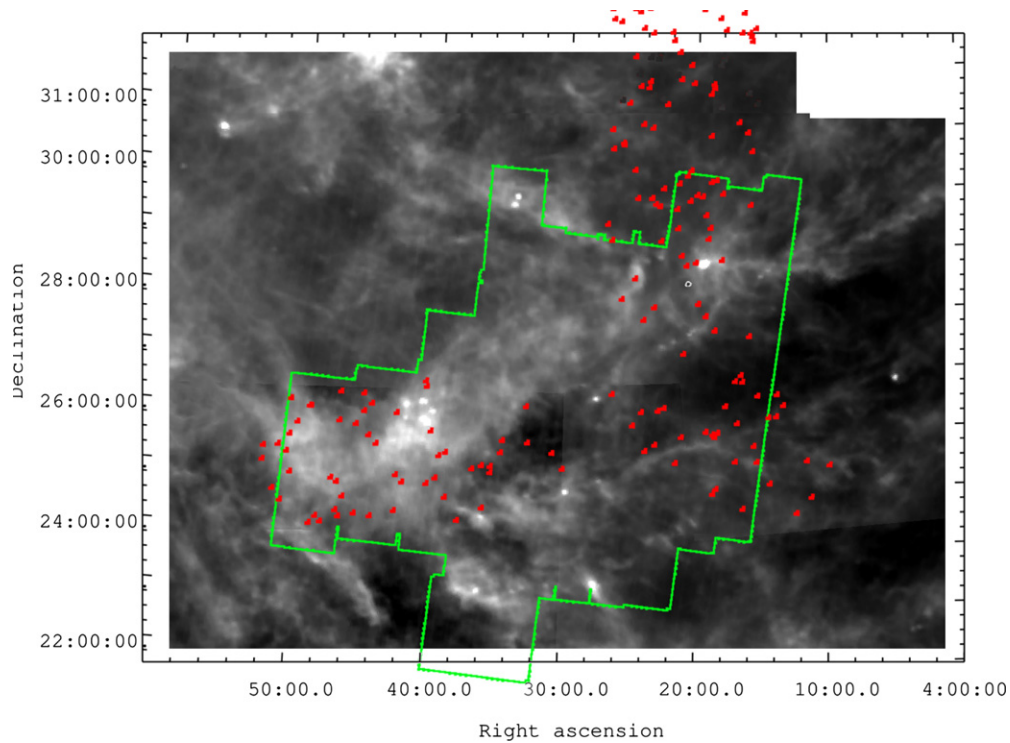
Figure 2. Areal extent of the Spitzer Taurus Legacy Survey (green) and SDSS spectroscopic observations by Knapp et al. 2007 (red symbols) overlaid on a mosaic of the Taurus region at $100\,\mu$m from the IRAS Sky Survey Atlas.

(A color version of this figure is available in the online journal.)

and IR photometric surveys is also only partial. We now describe the collation of data from each of the four sources.

First, to select early-type stars from SIMBAD, we used the criterion query: $ra > 60\ \&\ ra < 75\ \&\ dec > 22\ \&\ dec < 31\ \&\ sptypes < A0$. This query (run in early 2011) resulted in 91 stars, 3 of which were listed twice with different names. We thus obtained 88 B stars and zero O stars through the SIMBAD database as candidates.

Second, potential Taurus members having early spectral types were taken from Tables 5 and 7 in Rebull et al. (2010). One of these, JH 225, also resulted from the SIMBAD search. Thus, the Rebull et al. (2010) paper added eight more stars with spectral types early A or B (O-type stars were absent). As noted above, the region covered by *Spitzer* does not encompass the whole region of our search (see Figure 2).

Third, we selected from the 2MASS-PSC[7] objects satisfying the same coordinates constraint used in the SIMBAD query, having $K_s < 10$ mag with $>5\sigma$ detection, and no contamination or quality flags set. The brightness threshold places an upper limit on the visual extinction for the selected stars. For example, a B8V star can have a maximum visual extinction of $A_V \simeq 37$ to be selected, since the absolute K-band magnitude for such a star is $M_{K_s} = 0.11$, the distance modulus at 140 pc is 5.73, and the reddening law for 2MASS magnitudes is $A_K = 0.112 A_V$. Such a large value of extinction is much higher than the largest extinction observed for known Taurus members. The resulting 2MASS-PSC sample appears in the lower panels of Figure 3. These objects were further filtered through the photometric color criterion: $J - H < 1.698(H - K_s + 0.158)$ in order to select stars which, when translated backward on the reddening vector in the $(J - H)/(H - K_s)$ color–color diagram, fall on the main

sequence earlier than spectral-type A0. For this procedure, we used intrinsic magnitudes from Kraus & Hillenbrand (2007), and the Rieke & Lebofsky (1985) reddening law, which is found to be consistent with reddening in the 2MASS photometric system (Maheswar et al. 2010). There is no a priori reason to believe that this color criterion unconditionally, due to one or more of the following reasons: (1) photometric errors could place stars within the reddening band employed in our selection; (2) the reddening law (parameterized by R_V) is different for different lines of sight toward Taurus (e.g., Dobashi et al. 2005); (3) stars of a given spectral type and luminosity class do not have unique photometric colors but tend to have a dispersion of astrophysical origin about the observed mean intrinsic value; (4) additional emission of non-photospheric origin could change the $J - H$ and $H - K_s$ colors, possibly making late-type stars with IR excesses look like earlier-type stars that are reddened; (5) stellar multiplicity is unaccounted for in our analysis. Nevertheless, using a more relaxed criterion is subject to the risk of selecting a large number of unreddened K- and M-type stars which lie across the reddening vector defined by our photometric color criterion. Using our color criterion, we obtained 113 stars for further consideration. Fourteen of the stars selected in this manner were already present in the SIMBAD list of known early-type stars (BD+23 607, HD 25487, V1137 Tau, HD 284228, HD 282240, HD 29259, 2MASS J04395574+2545020 = IC 2087-IR, HD 283845, HD 283952, HD 31353, HD 284941, HD 284012, HD 283751, HD 283794) and so we added 99 early-type candidates through this criterion, which we appended to the working list. We also add the famous star AB Aur at this point, which would pass our color-selection criteria but is formally excluded from our analysis based on 2MASS-PSC flags present at K_s band.

Last, we added to our early-type candidates list the stars from the Finkbeiner et al. (2004) survey belonging to our spatial

---

[7] Using the multi-object search form at the Infrared Science Archive (http://irsa.ipac.caltech.edu/)
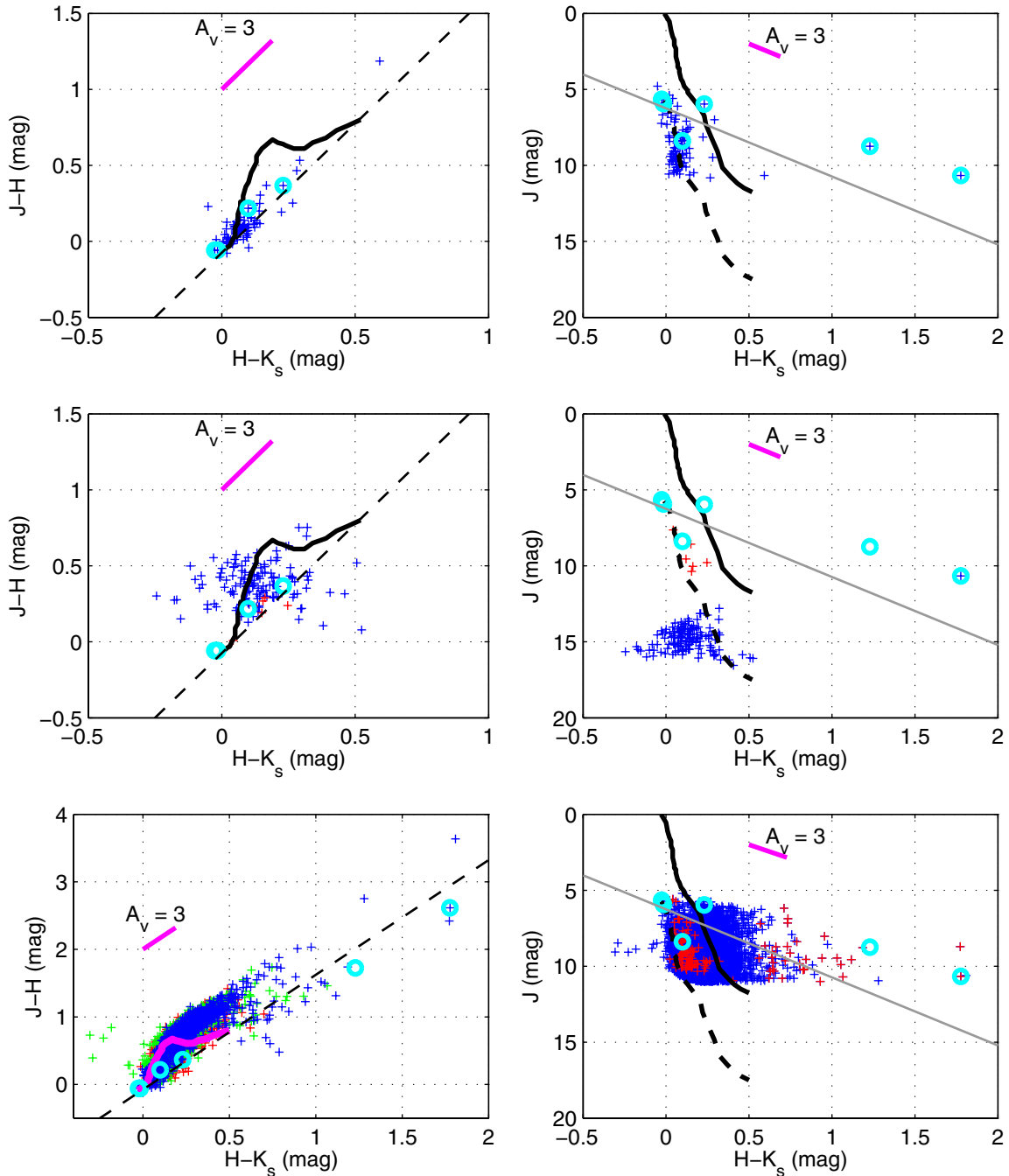
Figure 3. 2MASS color–color (left panels) and color–magnitude (right panels) diagrams for the early-type candidate stars considered in this work. 2MASS objects with contamination flags set and error in J, H, K_s magnitudes greater than 0.1 were rejected from the plots. The mean error in J, H, K_s magnitudes is about 0.02, which is smaller than the size of symbols used. Top panels: O, B stars from SIMBAD. In the color–color diagram, two of these stars lie outside the range plotted: V892 Tau (Elias 1) and IC 2087-IR, having $(H - K_s, J - H) = (1.23, 1.73), (1.78, 2.62)$, respectively. Middle panels: stars of spectral-type A and earlier from Knapp et al. (2007) are shown in blue. The B stars proposed by Rebull et al. (2010) are shown in red. Note that the area covered by these surveys is less than that represented in the top and bottom panels. Bottom panels: left—2MASS objects with color coding as follows. Blue: stars with magnitude $K_s < 8$, green: $8 < K_s < 9$, red: $9 < K_s < 10$. Right: all 2MASS objects are in blue, and those selected as possible O, B stars using the photometric selection criterion (described in Section 2.2) are shown in red. All panels: the reddening vector (magenta) from Rieke & Lebofsky (1985) is used. Intrinsic colors and magnitudes of main-sequence stars (from Table 5 of Kraus & Hillenbrand 2007) are shown as a thick black curve (magenta curve in the bottom panel color–color diagram). The thick black, dashed curve in color–magnitude diagrams is the same curve, but displaced along the luminosity axis to denote the apparent magnitude of main-sequence stars at 140 pc. The thin black, dashed straight line in the color–color diagrams represents the color-selection criterion applied to the 2MASS objects (see Section 2.2). The thin gray solid line in color–magnitude diagrams represents the reddening vector passing through the position of an A0V star at a distance of 140 pc. The location of the six B stars illuminating bright IR nebulae is shown as cyan circles with two of the stars having very similar, near-zero, colors.

(A color version of this figure is available in the online journal.)

region of interest which are classified as spectral class O, B, or A based on low-resolution SDSS spectra. Finkbeiner et al. chose the program stars for spectroscopy as those meeting one of two criteria: on the basis of red colors, as part of

a survey seeking M dwarfs, or as stars previously known as spectral class A or F, for use as reddening standards. As noted above, the region covered by SDSS does not encompass the whole Taurus cloud (see Figure 2). Furthermore, there was no

Table 2
Distances to Known Taurus Members Measured through VLBI Techniques

Star	α_{J2000} (h,m,s)	δ_{J2000} ($\circ$,$'$,$''$)	Distance (pc)	Ref.
HDE 283572	04 21 58.847	28 18 06.51	128.5 ± 0.6	1
V773 Tau	04 14 12.922	28 12 12.30	131.4 ± 2.4	2
V1023 Tau (Hubble 4)	04 18 47.037	28 20 07.32	132.8 ± 0.5	1
T Tau	04 21 59.434	19 32 06.42	146.7 ± 0.6	3
HP Tau/G2	04 35 54.152	22 54 13.46	161.4 ± 0.9	4

References. (1) Torres et al. 2007; (2) Torres et al. 2012; (3) Loinard et al. 2007; (4) Torres et al. 2009.

overlap between these candidates and those already selected above. We also considered a set of stars selected, similar to the 2MASS-PSC query described above, as those having $K_s <$ 10 mag and blue colors within SDSS, specifically $u - g < 0$. This resulted in a short list of a few tens of objects, nearly all of which were known to SIMBAD already as early-type stars (and thus included already among our first set of candidates), or as late-type stars (with blue colors unexpectedly blue, likely indicative of hot companions).

In addition to the stars in the four samples considered above, HD 31305 (A0V) is a star which we found in the vicinity of Taurus–Auriga due to its early spectral type and proximity to the well-known Taurus member AB Aur, though it is not within the area of the *Spitzer* maps of Taurus.

Our final list of early-type candidates for membership in the Taurus region of recent star formation thus consists of 329 stars. The color–color and color–magnitude diagrams for these stars, separated by the selection method, are shown in Figure 3. We tested these objects for Taurus membership as described in the next subsection, after assembling the needed ancillary data.

For all objects in our list of candidate O, B, and A0 stars, we collected the following astrometric and photometric information. Proper motions were taken from the PPMXL catalog (Roeser et al. 2010), and trigonometric parallaxes from the *Hipparcos* catalog (Perryman & ESA 1997). *B*, *V*, and *R* magnitudes listed in the NOMAD-1 catalog (Zacharias et al. 2005), and *J*, *H*, K_s magnitudes from 2MASS-PSC were used. Radial velocity (RV, heliocentric) information was extracted from Gontcharov (2006) and Kharchenko et al. (2007) in that order of priority. For the SDSS stars which we chose from Finkbeiner et al. (2004), we used an A0 template to extract their RVs using the SDSS DR7 (Abazajian et al. 2009). In each of these catalogs, we searched for counterparts to our early-type candidate stars within 1 arcsec of the source position. In cases where two counterparts were found for a particular source, only the closest was considered. Finally, the spectral types were adopted from our own derivations for those stars which we followed up spectroscopically (see Section 2.4), from Rebull et al. (2010) for stars listed in that paper, from SIMBAD, or from the ASCC-2.5 catalog (Kharchenko & Roeser 2009), in that order of preference. We also performed a thorough literature search, seeking relevant data not available through large catalogs.

2.3. Selection of Candidate Members of Taurus

Physical association of astronomical objects can be established through the combination of common location and common space motion, without all six dimensions available for every star. The case at hand is that of a star-forming region lying at a mean distance of 140 pc and having a depth and transverse
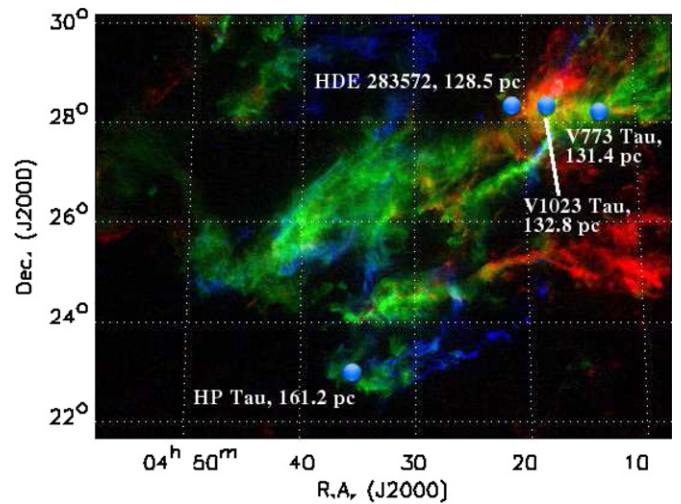

Figure 4. Distances to stars in Taurus measured via VLBI, from Table 2; the star T Tau is not shown since it lies south of the region of interest. Background image is velocity-coded ^{12}CO map from Goldsmith et al. (2008). The LSR velocities are color-coded as blue: 3–5 km s^{-1}, green: 5–7 km s^{-1}, red: 7–9 km s^{-1}.

(A color version of this figure is available in the online journal.)

extent of $\gtrsim 20$ pc. Although kinematics traditionally has been a robust mode of identification of cluster members, uncertainties in distance may lead to discrepant space velocities. Furthermore, the dispersion in the measured distance or kinematic quantities might be a significant fraction of their absolute values. With these challenges in mind, we chose the following filters to select (probable) members from our list of candidate early-type stars toward Taurus.

One set of criteria involved distance. Stars with trigonometric or spectroscopic parallax between 128 and 162 pc within 1σ error bar were considered. Another set of criteria involved kinematics. From the probability associated with a calculated χ^2 statistic, stars having proper motion consistent with known members were selected. Finally, RV was taken into account wherever available, considering as members stars with $9.8 \leqslant$ RV $\leqslant 17.5$ km s^{-1}, which incorporates the mean RVs of all Taurus groups identified by Luhman et al. (2009) within 1σ uncertainty.

2.3.1. Distance Criterion and Methods

Through VLBI measurements, the distances to five Taurus members are accurately known (see Table 2 and for context Figure 4). Taurus is at least as deep as it is wide (Torres et al. 2009), a few tens of parsecs in each direction. Based on this, we assume that Taurus occupies the region between 128 to 162 pc (i.e., $6.2 < \pi < 7.8$ mas on parallax). From our list of early-type candidate stars, we chose candidate Taurus members such that both their *Hipparcos* and spectroscopic parallax distances, within 1σ error, were consistent with the above-stated distance criterion. van Leeuwen (2007) has effectively demonstrated the validity of the *Hipparcos* parallaxes (however, see below for an argument against in the case of HD 26212). We calculated the spectroscopic parallax distances for each of the six magnitudes (denoted by "X" below)—*B*, *V*, *R*, *J*, *H*, and K_s—using the definition,

$$d_X = 10^{(X - A_X - M_X)/5} \times 10, \tag{1}$$

where $A_X = [B - V - (B - V)_0] \cdot R_V \cdot (A_X/A_V)$, $R_V = 3.1$, and $(A_X/A_V) = a + b/R_V$. The parameters "a" and "b" are from Table 3 of Cardelli et al. (1989), and are

the best-fit parameters to the average extinction law. M_V is from Schmidt-Kaler (1982), intrinsic colors, viz., $(B - V)_0$, $(V - R)_0$ are from Johnson (1966), and $(V - K)_0$, $(J - K)_0$, $(H - K)_0$ colors are from Koornneef (1983). The Koornneef magnitudes/colors were transformed into the 2MASS JHK_s system using transformations from Carpenter (2001). This intrinsic color and magnitude information for O-, B-, and A-type stars were compiled from Schmidt-Kaler (1982), Johnson (1966), Koornneef (1983), and Carroll & Ostlie (2006). BVR reddening was determined using Cardelli et al. (1989) with $R_V = 3.1$, and JHK_s reddening using Rieke & Lebofsky (1985). Stars with missing luminosity class information were assumed to be dwarfs. Candidates having spectral types for which the intrinsic magnitudes and colors are missing in our compiled tables necessitated interpolation between the two adjacent spectral types.

We note that the difference in spectroscopic parallax calculated using alternate color tables such as those of Schmidt-Kaler (1982), Fitzgerald (1970), or Johnson (1966) is less than 0.5%. More modern empirical color references that include both dwarfs and giants are rare and possibly non-existent. However, considering the tables of Pickles (1998; based on synthetic photometry from stitched together spectrophotometric data) or Bessell et al. (1998; based on synthetic photometry from model atmospheres), the spectroscopic parallax differences are larger, but less than 3%. A more worrisome discrepancy lies in the absolute V-band magnitude, M_V, where the Pickles (1998) results differ from the Johnson (1966) values used in our compilation by 0.5–1 mag, leading to 5%–50% disagreement in the spectroscopic parallaxes. However, at least for B-type stars, the M_V from Johnson (1966) agrees with observations of well-studied stars (e.g., the 100 brightest stars[8]) better than does the Pickles (1998) scale; Bessell et al. (1998) do not quote M_V.

The error reported on the spectroscopic parallax distance is the standard deviation of the distances calculated using magnitudes at all of the six different wavelengths. As well-tested empirical estimates of intrinsic colors involving R, J, H, and K_s are not available for early-type giant stars, we calculate the distance to the luminosity class III stars using only B, V magnitudes and color. Other errors that could contribute but have not been accounted for include: (1) spectral type/luminosity classification error, (2) error in apparent magnitudes, (3) intrinsic colors are mean values and do not account for astrophysical spread within the luminosity classes, (4) error in choice of reddening model, and (5) the presence of non-photospheric emission such as IR excess. For points (1) and (2) stated above, the manner in which these criteria impact the distance estimate can be understood quantitatively via the discussion provided in Section 3.3 of Kenyon et al. (1994). Following that discussion, the 1σ error on spectroscopic parallax corresponding to quantities (1) and (2) is roughly 30 pc at a spectral type of A0 with $d = 140$ pc. This uncertainty would then add to our quoted error appropriately taking into account Equation (1). Caution is thus advised in using the error bars quoted on spectroscopic distances, especially for giant stars.

Out of the 329 early-type candidates being tested for Taurus membership, the reddening and spectroscopic parallax distance can be calculated for 173 of them. In general, where there is overlap, the reddening values show good agreement with those stated in the literature. We compare our averaged spectroscopic parallax distances with those determined by Kenyon et al. (1994), Walter & Boyd (1991), Lesh (1968), and Blaauw (1956)
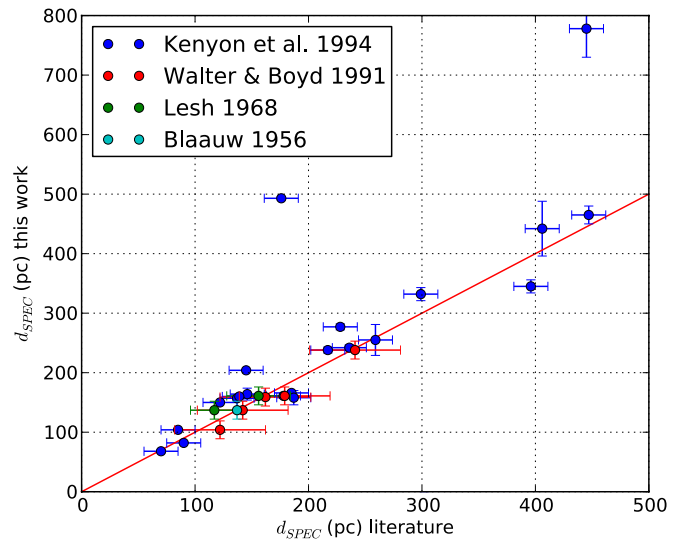
Figure 5. Comparison of spectroscopic distances calculated in this work with those published in past literature.

(A color version of this figure is available in the online journal.)

in Figure 5. For the majority of the objects, the spectroscopic parallax distances are in agreement within 1σ with those determined by *Hipparcos*. Notable exceptions are stars with very high reddening for which R_V (and possibly also the reddening law as a function of wavelength itself) would differ significantly from the value assumed here. Also, the method fails if the optical and/or near-IR photometry is dominated by circumstellar rather than photospheric emission, or if the source is pre-main sequence rather than close to the main sequence; this latter condition is indeed the case for many of the later-type stars selected in the 2MASS part of the search.

In considering the appropriateness of the distance criterion we have adopted for testing the association with Taurus, which is that all stars must lie between 128 and 162 pc, a problem arises in the unknown three-dimensional shape of the molecular cloud. The cloud may extend further along some lines of sight, or it may not have high enough density for current star formation along other lines of sight. A related problem in establishing membership is that to the west of Taurus, there is another star-forming region along the line of sight extending behind Taurus: the Perseus molecular cloud at about 350 pc. The spectroscopic parallaxes of HD 282276 and HD 283677 suggest that they both lie closer to the Perseus cloud, though on the sky they are aligned with Taurus, not the Perseus cloud; these stars also have similar proper motion (see below). There have been suggestions of a bridge of molecular material connecting the Taurus–Auriga and Perseus regions (Ungerechts & Thaddeus 1987). The presence of the somewhat older Cas-Tau OB association along the line of sight also poses a potential contamination problem because its members span a range of at least 30 pc in distance (de Zeeuw et al. 1999) and perhaps as much as 80 pc, although it is securely behind the Taurus star-forming region.

A method for distinguishing chance superpositions, in addition to the distance criterion, is to look at the kinematics of the stars and the natal cloud. Consideration of the proper motion and RV of the stars helps in eliminating ambiguity, as discussed in the next subsection.

2.3.2. Kinematic Criteria and Methods

The classical studies of proper motions of stars in the vicinity of the Taurus clouds are those of Jones & Herbig (1979) and

Hartmann et al. (1991), with Ducourant et al. (2005) providing the latest catalog for Taurus. Kinematic membership probabilities are typically based on the convergent-point method, which is used for regions that cover a large part of sky where the mean subgroup motion is changing as a function of position (this is a purely geometric effect). For regions less than a few degrees in size in the vicinity of comoving groups in Taurus, one can test the consistency of the proper motion of one star simply with respect to the mean motion of a group. Luhman et al. (2009) computed the mean proper motions and RVs of 11 distinct groups (occupying 1–10 deg^2 on the sky; see Table 8 of that paper) of Taurus members. Seven of these groups, specifically I–V, VIII, and X, lie within our region of interest.

We checked the statistical consistency between the proper motion of the candidate early-type stars reported in Table 3 and the proper motion of the closest kinematic group from Luhman et al. (2009) by estimating the χ^2 probability. The two components of proper motion, μ_α and μ_δ, can be understood as independent Gaussian variates drawn from a normal distribution parameterized by the mean (which can be estimated through the sample mean, i.e., the mean proper motion of the presently known Taurus members) and the dispersion (likewise estimated as the dispersion of the sample of presently known Taurus members). The sum of the square of these values will then be distributed according to the χ^2 distribution. Strictly speaking, these components are determined through the least-squares technique in proper-motion catalogs, and are correlated (the complete covariance matrix is, for example, provided by the *Hipparcos* catalog). Here, we have calculated the quantity χ^2 using the definition $\sum_{i=1}^{k}(x_i - \bar{x})/\sigma_i^2$, where $i = 1, 2$, and x_i describes the components of proper motion. The uncertainties, however, are associated with not only the proper motion of individual stars, but also with the sample mean. Furthermore, we have to incorporate the internal dispersion of the presently known members of Taurus. We calculated the χ^2 statistic and the associated probability using Equations (2) and (3), after de Zeeuw et al. (1999):

$$\chi^2_{\nu=2} = \frac{(\mu_\alpha - \mu_{\alpha,\mathrm{group}})^2}{(\sigma^2_{\mu_\alpha} + \sigma^2_{\mathrm{int}} + \sigma^2_{\mu_{\alpha,\mathrm{group}}})}$$
$$+ \frac{(\mu_\delta - \mu_{\alpha,\mathrm{group}})^2}{(\sigma^2_{\mu_\delta} + \sigma^2_{\mathrm{int}} + \sigma^2_{\mu_{\delta,\mathrm{group}}})} \quad (2)$$

$$P(\chi|\nu) = \frac{\chi^{(\nu-2)/2}e^{-\chi/2}}{2^{\nu/2}\Gamma(\nu/2)}, \quad (3)$$

where μ_α, μ_δ, σ_{μ_α}, σ_{μ_δ} denote the proper motion in right ascension and declination of the star being tested and their associated uncertainties. The quantities μ_{group}, $\sigma_{\mu_{\mathrm{group}}}$, σ_{int} are the proper motion of the Taurus group closest to the star, its uncertainty, and the intrinsic dispersion of proper motion in the group (assumed to be 2 mas yr^{-1}). The denominator of each term is then the expected variance of the respective numerators. This method traditionally has been used to find "proper-motion members," but is partly biased toward stars having a large relative uncertainty in their proper motion which reduces the χ^2. We are able to calculate the χ^2 probability for all of the 329 early-type candidate stars being tested for Taurus membership.

The result of this proper-motion analysis is illustrated in the upper panel of Figure 6. The region allowed by our χ^2 probability membership criterion (set at >1%) roughly corresponds to the shaded circular region. In the context of this
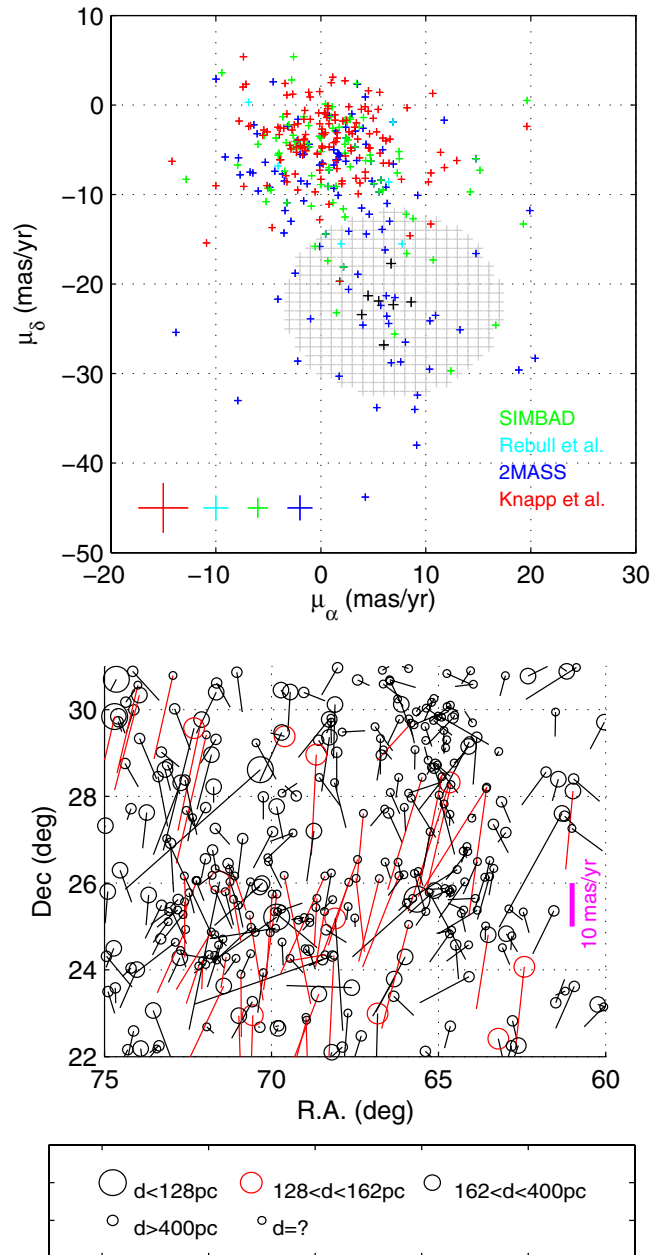

Figure 6. Upper panel: proper motions of the candidate early-type stars shown as a cloud plot with blue indicating objects selected from 2MASS; green, SIMBAD; cyan, the B stars proposed by Rebull et al. (2010); and red, the O, B, A stars from Knapp et al. (2007). The "+" symbols at the bottom-left corner denote the mean errors for each sample. The mean proper motion of Taurus groups considered in this paper (see Section 2.3.2) is shown as black symbols. The hatched reference circle indicates the area where the χ^2 probability of membership is greater than 1% with respect to the mean proper motion of Taurus. Fifty-one stars from our list of candidate early-type stars have proper motions consistent with Taurus groups. Lower panel: vector diagram showing the proper motion of all the stars tested for membership. Those which satisfy the proper-motion criterion $P(\chi^2 > 1\%)$ are shown in red. Positions of the stars are indicated by the circles, whose sizes are based on the spectroscopic parallax distance of the respective stars (key given at the bottom). The red circles denote stars satisfying our distance criterion for Taurus member selection (within an uncertainty of 15 pc).

(A color version of this figure is available in the online journal.)

figure, it is worthwhile to note that members of the background Cas-Tau OB association as listed by de Zeeuw et al. (1999) have μ_α ranging from a few mas yr^{-1} to 50 mas yr^{-1} (the mean is about 26 mas yr^{-1}), and μ_δ ranging from a negative few mas yr^{-1} to -40 mas yr^{-1} (mean is about -19 mas yr^{-1};

Table 3
List of Candidate Early-type Stars with Sections Separating Various Selection Methods

B#	Star	α	δ	d_{HIP}	d_{SPEC}	$\mu_\alpha \cos\delta$	μ_δ	RV	SpT	Candidate?	
		(ICRS 2000, deg)			(pc)	(mas yr^{-1})		(km s^{-1})		d	μ/RV
					O, B, and A0 stars from SIMBAD						
1	HD 25063	60.036389	29.710836	$\cdots$	195 ± 5	3.7 ± 0.9	-6.2 ± 0.8	$\cdots$	B9	N	N/?
2	HD 25201	60.236744	23.201484	332^{+274}_{-103}	189 ± 5	-34.6 ± 15.2	-9.2 ± 15.2	13.8 ± 1.1	B9V	N/N	N/Y
3	HD 281490	60.871667	30.970278	$\cdots$	792 ± 123	13.0 ± 1.6	-7.3 ± 1.7	$\cdots$	B9/A3	N	N/?
					Additional B and early A stars proposed by Rebull et al. (2010) from infrared excess						
89	HD 27659	65.727746	28.398614	$\cdots$	164 ± 10	-23.7 ± 1.5	-17.8 ± 1.4	$\cdots$	A3V	Y	N/?
90	HD 27923	66.329861	23.788020	194^{+101}_{-49}	277 ± 5	5.9 ± 1.1	-8.6 ± 1.1	$\cdots$	B9V	Y/N	N/?
91	HD 283637	66.495250	27.617028	$\cdots$	855 ± 279	-3.6 ± 1.7	-6.8 ± 1.7	$\cdots$	B9.5V	N	N/?
					Additional early-type candidates selected from 2MASS photometry						
97	HD 25111	60.054439	23.149068	$\cdots$	$\cdots$	5.4 ± 1.1	-4.6 ± 1.1	$\cdots$	A	?	N/?
98	HD 283286	60.959556	28.404501	$\cdots$	420 ± 21	-6.9 ± 2.7	-5.19 ± 2.37	$\cdots$	A2	N	N/?
99	04040178+2715454	61.007451	27.262593	$\cdots$	$\cdots$	-8.1 ± 5.6	-5.16 ± 4.98	$\cdots$	?	?	N/?
					O, B, A stars from Knapp et al. SDSS data						
196	04095167+2520112	62.465271	25.336500	$\cdots$	4389 ± 605	-1.6 ± 3.7	-4.8 ± 3.7	-0.1 ± 1.6	A0	N	N/N
197	04111342+2447170	62.805889	24.788080	$\cdots$	8576 ± 2737	0.3 ± 3.8	-3.3 ± 3.8	37.5 ± 3.2	A0	N	N/N
198	04113476+2524136	62.894859	25.403830	$\cdots$	12774 ± 2784	-3.7 ± 4.3	-2.5 ± 4.3	-2.5 ± 2.5	A0	N	N/N
					Other stars						
328	HD 31305	73.950958	30.337911	$\cdots$	174 ± 11	6.4 ± 1.7	-21.9 ± 1.6	$\cdots$	A1V	N	Y/?
329	HD 31293	73.941022	30.551191	139^{+22}_{-16}	121 ± 50	1.9 ± 0.9	-24.4 ± 0.7	8.9 ± 0.9	$\sim$A0V	Y	Y/Y

Notes. (1) Error on d_{SPEC} is the standard deviation among distances calculated using B, V, R, J, H, and K magnitudes, as available, and underestimates true error values; see the text. (2) Errors on other columns are taken from original references; see the text. (3) Spectral types are from SIMBAD and Kharchenko & Roeser (2009) in the top three sections, with a slash (/) denoting any discrepancy between these two compilations, and from SDSS in the fourth section. In cases where we have derived new spectral types ourselves in this paper (see Table 4), our types supersede those from the references. (4) Last two columns state whether or not (Y/N) the star is a probable Taurus member based on the two distance estimates (d), and the two kinematic assessments: proper motion (μ) and radial velocity (RV); see the text.

(This table is available in its entirety in a machine-readable form in the online journal. A portion is shown here for guidance regarding its form and content.)

from the PPMXL catalog). Thus, a few of the stars studied herein are probably Cas-Tau members. A combined diagram showing the spectroscopic parallax distance and the proper motion of the early-type candidate stars is shown in the lower panel of Figure 6.

The RV dimension was not included in the χ^2 analysis because this quantity is unknown for most stars. In cases where it is known, the uncertainties are generally quite large. Thus, as the second component of our kinematics investigation, we compared the RV of each of the early-type candidate member stars (where available and as reported in Table 3) with that of the nearest Taurus group listed in Luhman et al. (2009). We chose as likely members the stars which, within 1σ, satisfied the criterion $9.8 \leqslant$ RV $\leqslant 17.5$, corresponding to the range in the mean RVs of the Taurus groups. For the SDSS-selected early-type stars, we show the RVs in Figure 7. Most of the SDSS-selected stars satisfying the nominal RV-selection criterion are too faint in the near-IR to be probable members of Taurus.

2.3.3. Results of Candidate Selection

The information in Table 3 was used along with the procedures outlined above to arrive at the list of likely early-type members of Taurus. In all, 52 stars independently satisfy the proper-motion membership criteria and 28 the distance membership criteria, with 18 satisfying both. However, not all sources have known values for all or any of the quantities we consider. As the samples of early-type stars under consideration were derived from four different sources, we discuss the details of our analysis as appropriate for each sample in what follows.

For the SIMBAD sample of known early-type stars and for the Rebull et al. IR excess sample, spectral types exist in
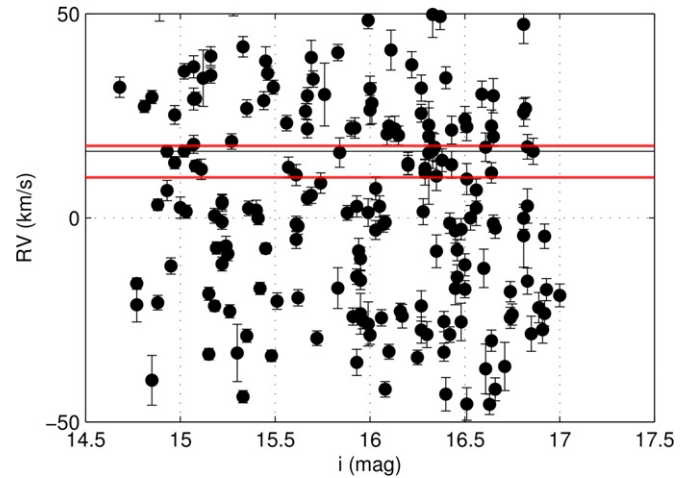

Figure 7. Radial velocity vs. SDSS i-band magnitude for the early-type stars selected from Knapp et al. (2007). The y-axis has been rescaled to show only the stars with RV between ± 50 km s^{-1}. The mean RV of accepted members of Taurus (Luhman et al. 2009), 15.8 km s^{-1}, is shown with a black horizontal line. The neighboring red lines denote the region $9.8 \leqslant$ RV $\leqslant 17.5$, our RV-member selection criterion. No concentration at the Taurus velocity is seen, and among those stars satisfying this RV criterion, most are too faint to be probable members of Taurus.

(A color version of this figure is available in the online journal.)

the literature. Also, we have followed up some of these stars spectroscopically ourselves in order to verify or revise their spectral classification. Fairly accurate spectroscopic parallax distances have thus been used to test the membership of these two sets of stars with Taurus. RV measurements also exist for some of these stars. We found that two stars, HD 28929 (B8V,

also known as HR 1445) and HD 29763 (B3V, also known as τ Tau), satisfy all the tested criteria for membership of Taurus: parallax distance, proper motion, and RV. V892 Tau (A0, also known as Elias 1) satisfies the first two criteria, leaving the third unknown due to insufficient information, but this star is already an accepted member of Taurus on the basis of its circumstellar disk attributes.

In the 2MASS photometric sample, accurate spectral classification is absent for many of the stars, and calculation of accurate spectroscopic parallax has not been possible for these. In this set of stars, 12 satisfy two criteria leaving the third criterion indeterminate due to insufficient information, while 2 stars satisfies all the criteria for membership of Taurus. However, many of these stars are late-type T Tauri stars that are already known members of Taurus but are selected by our methods because they have large enough near-IR excesses to push them into the region of the 2MASS color–color diagram occupied by reddened earlier type stars. We note that the 2MASS search does select the mid-A stars HD 26212 and HD 31648 (along with AB Aur, if we ignore the 2MASS-PSC flag at K_s band) as candidate early-type members, but finds no new B stars.

For the SDSS spectroscopic sample, the magnitude range precludes the availability of any *Hipparcos* parallax values, but since spectral types are available for many stars, spectroscopic parallaxes can be calculated. RV is also measured by the SDSS analysis pipeline. Some of the SDSS-selected stars satisfy the kinematic criteria (see Figures 6 and 7); however, they are underluminous with respect to the expectations for reddened early-type stars at the Taurus distance (see middle panels of Figure 3) and indeed have much larger spectroscopic distance estimates (Table 3). Most of these early-type stars are likely in the Galactic halo.

Finally, the spectroscopic parallax distance suggests that HD 31305 (located near AB Aur and discussed by Cody et al. 2013) lies just beyond the distance range defined by our member-selection criterion ($<10\%$ in excess of the standard deviation among calculated d_{SPEC} values). Nevertheless, its proper motion conforms with that of known Taurus members. Hence, we consider in what follows that this star could well be a member of Taurus.

In summary, we newly advocate the membership of two B-type stars (HD 28929 and HD 29763) and one A-type star (HD 26212) in Taurus using distance and kinematic arguments, and in addition find one A0-type star (HD 31305) to be a probable member (though it is not yet confirmed due to the lack of RV information). Below, in Section 3, we discuss these stars in more detail and also revisit some of those which were rejected in the above procedures. After consideration of other evidence which might point toward their association with Taurus, we find several additional B and A0 types to be plausible Taurus members. In order to inform our further assessments regarding the likelihood of cluster membership, additional data on many of these stars were collected.

2.4. Follow-up Spectroscopy

We performed follow-up spectroscopy of selected stars with an aim of (1) confirming or revising their spectral types based on temperature and surface gravity diagnostics, (2) measuring RVs, and (3) determining more precise stellar parameters so as to estimate ages. We obtained optical spectra for a subset of the Taurus early-type candidates which were found to satisfy several of our membership criteria, or which illuminated a nebula in the *Spitzer* image. Some of these sources appeared to be better

candidates at the time we obtained the spectra than later re-analysis revealed. We also observed for comparison a grid of dwarf B stars from Abt et al. (2002), and, for calibration, RV standard stars and spectrophotometric standards.

The optical spectra were obtained at the Palomar 200 inch Hale telescope on 2010 December 4 using the Double Spectrograph (DBSP). The data have medium spectral resolution ($R \simeq 7800$ and 10,419 in the blue and red channels, respectively). We used a dichroic at 5500 Å to split the optical light into blue and red channels with a 1200 lines mm^{-1} grating blazed at 4700 Å, at a grating angle 34°92 on the blue side and 1200 lines mm^{-1}, 7100 Å blaze, and 42°73 on the red side. The spectral range covered was $\sim$3480–5020 Å at 0.55 Å pixel^{-1} (blue) and $\sim$6440–7110 Å at 1.4 Å pixel^{-1} (red). For wavelength calibration, we used an Fe–Ar lamp in the blue and an He–Ne–Ar lamp in the red. Spectra for two stars (HD 27659 and HD 26212) were taken on 2011 September 2 using a different configuration resulting in a much lower resolution and a larger wavelength coverage.

We reduced the data using the Image Reduction and Analysis Facility (IRAF) *ccdred* and *onedspec* packages. Spectra were extracted with the *apall* task after trimming, bias-subtraction, and flat fielding of the images. The wavelength solution was then applied using *dispcor*. In the case of stars for which we had multiple short-exposure observations, the spectra were coadded using *scombine* to get a higher signal-to-noise ratio. We normalized all the spectra with *splot*.

For spectral typing the program stars, we measured the equivalent widths of several diagnostic absorption lines using *splot*, and then compared them with those of reference-grid stars (Figure 8), guided by the graphics in Didelon (1982). The normalized spectra of the reference-grid stars and the program stars are shown in Figure 9 with the reference types adopted from the literature and the program star types derived by us. We also compared our spectra with templates by Gray[9] and Morgan et al. (1943).[10] The results of the spectroscopic analysis are given in Table 4. Estimates for the effective temperature (T_{eff}), projected rotational velocity ($v \cdot \sin i$), and the surface gravity ($\log g$) were made by fitting the spectra with templates from Munari et al. (2005). For the template spectra, the comparison grid resolution was 500–1000 K in T_{eff} and 0.5 in $\log g$, while the grid in $v \cdot \sin i$ was: 0, 10, 20, 30, 40, 50, 75, 100, 150, 200, 250, and 300 km s^{-1}; hence, our derived values are no more accurate than this. Some stars have equally good fits between a higher temperature and gravity point, versus a lower temperature and gravity point one grid spacing away; in these cases, we generally preferred the dwarf to the giant solution. The physical parameters derived from this fitting are given in Table 5. In combination with the set of intrinsic stellar parameters discussed above, we thus derived a second set of spectral types for the stars that were spectroscopically followed up. These spectral types generally agree with those derived using equivalent widths in Table 4. Due to the coarse spectral grid of templates and degeneracies involved in the fitting process, the spectral types derived from our equivalent width analysis usually take precedence over those derived from spectral fitting.

Unfortunately, RV information could not be derived from our spectra at the expected performance of the instrument (given our care in taking source-by-source comparison lamp calibration frames), perhaps due to poorly understood flexure effects. We

---

[9] http://ned.ipac.caltech.edu/level5/Gray/Gray_contents.html
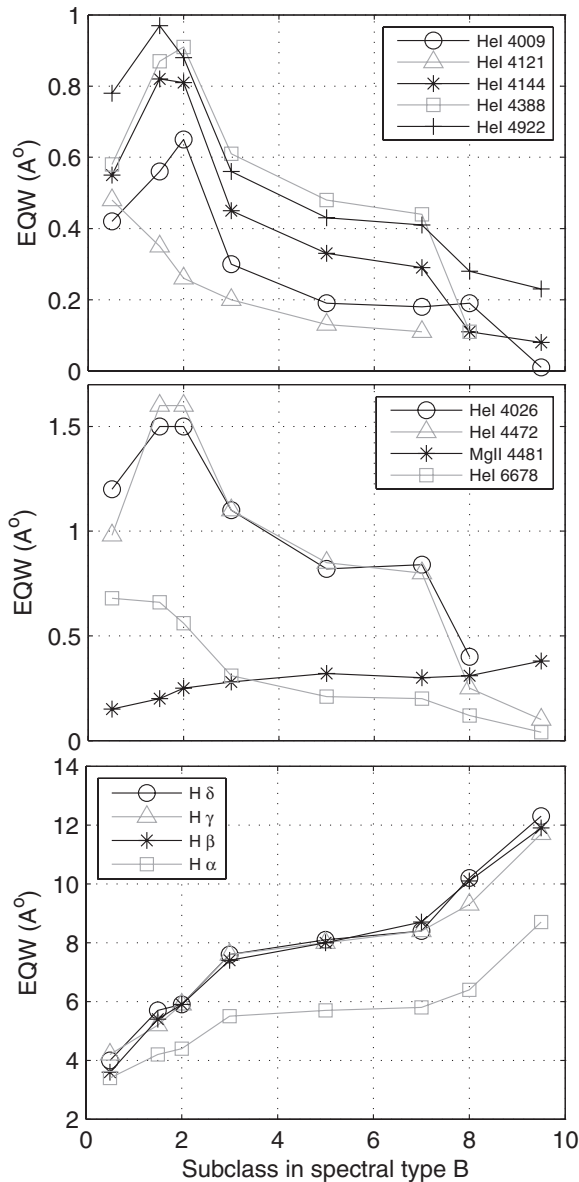[10] http://ned.ipac.caltech.edu/level5/ASS_Atlas/MK_contents.html

Figure 8. Equivalent widths of various absorption lines measured in the grid of B-type spectral standard stars (luminosity class V only) that were observed for comparison with the Taurus candidate early-type stars.

note that an error as small as 1 Å in the wavelength calibration leads to an error of about 66 km s^{-1} at 4500 Å. Shifts of this order have been experienced between contiguous exposures while working with DBSP data. Due to our short-exposure times, there are no sky lines in the blue part of the spectrum that could aid in more accurate wavelength calibration. While the red channel spectra have ample telluric absorption, too few photospheric absorption lines are available to provide a good fit. Hence, we defer the estimation of RV to a later time with another data set.

Notably, hydrogen emission lines or line cores are seen in HD 283751, HD 283637, V892 Tau, and AB Aur (see Figure 9). While the emission properties of the last two stars in this list are well known, they have not been reported previously for the first two objects. Emission lines are often taken as a signature of activity associated with stellar youth, although evolved early-B-type stars may exhibit a "Be phenomenon." We note that the derived spectral types of these emission-line objects are B5e and B9.5e, later than typical of evolved Be stars, but the IR excesses detected by Rebull et al. (2010) are more typical of evolved Be

stars than of young accretion disk systems. Neither star can be associated with Taurus by kinematic or distance arguments, and thus they appear to be interesting background interlopers.

A further note concerning the spectra is the appearance in Figure 9 of what is likely diffuse interstellar band absorption at 6614 Å in about half of the program stars. Corresponding broad absorption at 4428 Å is also seen. There is excellent correlation between the presence of this feature and the spectroscopic parallax distance estimates reported in Table 3. Distant stars have the absorption while closer stars do not. Notably, none of the stars we eventually conclude in this work to be associated with Taurus have these interstellar absorption features.

Finally, we call attention to ubiquitous absorption at 6708 Å, coincident with the Li I line seen in young low-mass stars, that is seen in all of our spectra taken on 2010 December 4 (Figure 9). The feature is not likely to be astrophysical and we suspect a (currently unexplained) terrestrial origin, perhaps related to a meteor shower.

2.5. Modeling the Dust Emission with DUSTY

In this section, we consider the nebular structures associated with several of the early-type sources and prepare to model in the next section their multiwavelength image morphology. Reflection nebulae appear bluish when illuminated by light from a nearby star on account of the scattering properties of dust. The star and the dust may be physically related, or the encounter between the star and a cloud of overdense ISM may be by chance. IR emission is also associated with the illuminated clouds, due to the warm dust, but compared to, e.g., H II regions, the IR luminosity is lower and there is a lack of radio emission.

DUSTY[11] solves the radiation transfer problem for a light source embedded in dust through an integral equation for the spectral energy density (Ivezic & Elitzur 1997). The code takes the following input parameters: type of external radiation source, dust composition, grain size distribution, dust temperature at the edge nearest to the external source, geometry of the cloud (spherical shell/planar slab), density profile, and the optical depth. The dust temperature and optical depth together define the amount of radiation present at the edge of the photodissociation region (PDR). Ideally, given the dust properties and parameters of the illuminating star, the inner temperature of dust can be calculated giving us the separation from the star. Following Tielens (2005), we can calculate the dust temperature in a slab geometry as

$$(T_d/\text{Kelvin})^5 = 2.7 \times 10^5 \, G_0 \, e^{-1.8 \, A_V}$$
$$+ 4.1 \times 10^{-4} \left[0.42 - \ln(4.3 \times 10^{-4} \, G_0) \, G_0^{6/5} \right]$$
$$+ 2.7^5, \qquad (4)$$

where A_V is the reddening caused by the slab. The assumption here is a simplistic model in which the absorption efficiency of the dust is directly proportional to the wavelength for $\lambda < \lambda_0 = 1000$ Å and is unity elsewhere; the dust size is $a = 1 \, \mu$m. G_0, the far-ultraviolet (FUV, $h\nu > 13.6$ eV) radiation field in terms of the average interstellar radiation field (1.6×10^{-3} erg cm^{-2} s^{-1}), is given by

$$G_0 = 1.8 \times \left(\frac{L_*}{100 \, L_\odot} \right) \left(\frac{\chi}{3.6 \times 10^{-4}} \right) \left(\frac{d}{0.02 \, \text{pc}} \right)^{-2}, \quad (5)$$

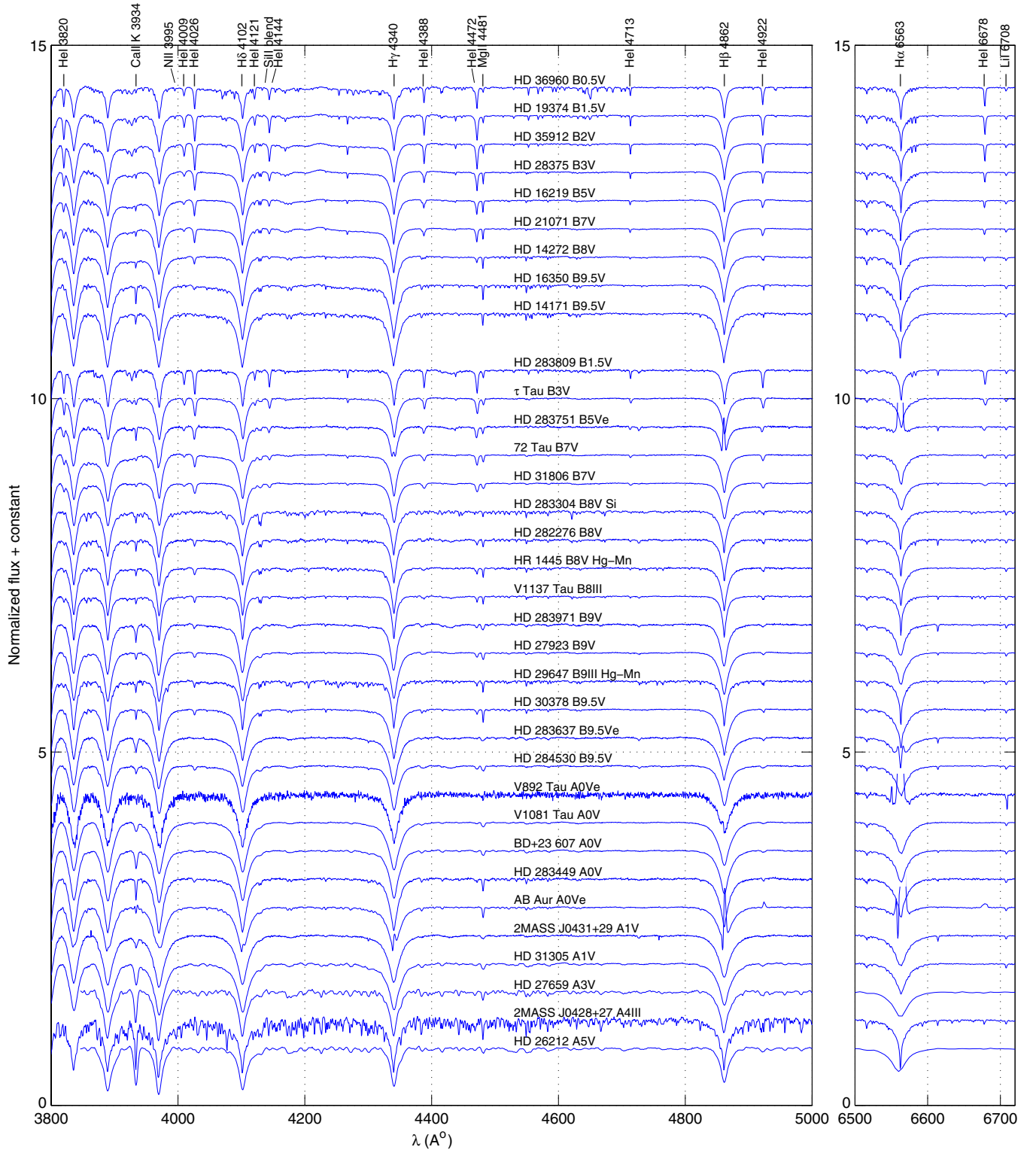[11] http://www.pa.uky.edu/~moshe/dusty/

Figure 9. Normalized optical spectra obtained at the Palomar 200 inch Hale telescope. The upper set of stars comprise the grid of B-type spectral standard stars used for assigning spectral types to the program stars (lower set of spectra). All spectra have an arbitrary offset along the ordinate. Note the hydrogen emission lines or line cores in HD 283751, HD 283637, V892 Tau, and AB Aur. Approximately half of the program stars have diffuse interstellar band signatures: a narrow absorption at 6614 Å and a broader shallow feature at 4428 Å. The feature labeled as Li I 6708 Å in the right panel is probably anomalous as this line is not expected to be present in these early-type young stars, and especially not in the spectral standards (including our white dwarf flux standard which is not shown); we suspect a possible terrestrial atmosphere source, perhaps associated with the Geminid meteor shower; this hypothesis is supported by lack of absorption at this wavelength in the two spectra toward the bottom of the sequence that were taken on a different night from all others.

(A color version of this figure is available in the online journal.)

Table 4
Spectral Types Derived through New Spectroscopy

B#	Star	S/N/100	Equivalent Widths																Derived SpT
			Ca II K 3933.7	N II 3995.0	He I 4009.3	He I 4026.2	Hδ 4101.7	He I 4120.8	Si II 4128.1, 4130.9	He I 4143.7	Hγ 4340.4	He I 4387.9	He I 4471.5	Mg II 4481.2	Hβ 4862.3	He I 4921.9	Hα 6562.8	He I 6678.2	
			Spectral-type standards																
	HD 36960	3.0	0.12	0.09	0.42	1.2	4.0	0.48	0.02	0.55	4.2	0.58	0.98	0.15	3.6	0.78	3.4	0.68	B0.5V
	HD 19374	2.6	0.15	0.08	0.56	1.5	5.7	0.35	0.08	0.82	5.2	0.87	1.6	0.20	5.4	0.97	4.2	0.66	B1.5V
	HD 35912	3.2	0.14	0.04	0.65	1.5	5.9	0.26	0.12	0.81	5.9	0.91	1.6	0.25	5.9	0.88	4.4	0.56	B2V
	HD 28375	2.6	0.13	0.01	0.30	1.1	7.6	0.20	0.21	0.45	7.6	0.61	1.1	0.28	7.4	0.56	5.5	0.31	B3V
	HD 16219	2.7	0.13	0.01	0.19	0.82	8.1	0.13	0.26	0.33	8.0	0.48	0.85	0.32	8.0	0.43	5.7	0.21	B5V
	HD 21071	2.7	0.14	<0.01	0.15	0.84	8.4	0.11	0.24	0.29	8.4	0.44	0.80	0.30	8.7	0.41	5.8	0.20	B7V
	HD 14272	1.7	0.19	...	<0.02	0.40	10.2	a	0.24	0.11	9.3	0.11	0.25	0.31	10.1	0.28	6.4	0.12	B8V
	HD 16350	1.9	0.57	...	...	a	12.3	a	0.26	0.08	17.8	a	0.10	0.38	11.9	<0.23	8.7	0.04	B9.5V
	HD 14171	1.7	0.29	...	...	...	14.6	a	0.30	a	13.0	...	0.023	0.33	13.6	a	9.4	a	B9.5V
			O, B, and A0 stars from SIMBAD																
50	HD 283809	1.8	0.24	0.09	0.70	1.4	4.9	0.35	0.10	0.86	4.9	0.90	1.4	0.27	5.0	0.93	3.8	0.64	B1.5-2V
51	τ Tau	2.4	0.29	0.01	0.43	1.2	8.2	0.21	0.15	0.56	7.9	0.72	1.0	0.27	7.8	0.68	5.6	0.38	B3V
25	72 Tau	3.1	0.12	0.02	0.16	0.82	9.8	>0.1	0.24	0.27	9.2	0.49	0.75	0.31	8.6	0.41	6.0	0.18	B7V
88	HD 31806	3.4	0.12	0.01	0.21	0.77	9.7	a	0.22	0.27	8.7	0.45	0.72	0.34	8.8	0.39	6.4	0.19	B7V
6	HD 283304	1.2	0.42	...	0.03	a	8.9	a	0.79	b	8.2	0.15	0.07	0.16	8.2	0.20	6.6	<0.05	B8V Si
33	HD 282276	1.4	0.28	0.02	0.05	0.31	8.9	b	0.41	0.09	8.2	a	0.29	0.26	8.0	0.24	6.5	0.12	B8V
36	HR 1445	2.3	0.19	bc	0.04	0.41	9.6	a	0.30	0.13	9.1	<0.20	0.32	0.32	8.7	0.26	6.7	0.05	B8V
13	V1137 Tau	2.9	0.18	0.01	0.11	0.29	6.4	>0.05	0.37	0.11	5.9	<0.22	0.30	0.22	6.5	0.22	5.9	0.09	B8III
48	HD 29647	1.6	0.31	0.04	<0.1	0.24	8.7	a	0.34	0.09	7.8	<0.19	0.26	0.39	7.7	0.22	6.1	0.06	B9III
81	HD 283971	1.6	0.92	0.01	0.03	0.25	11.1	a	0.25	0.07	9.5	a	0.19	0.38	10.6	<0.22	7.9	<0.05	B9V
63	HD 30378	3.0	0.28	<0.01	0.01	0.24	13.6	a	0.24	0.06	13.0	<0.1	0.27	0.44	12.7	0.18	9.1	<0.05	B9.5V
4	BD+23607	2.3	1.1	<0.01	b	<0.01	16.6	a	a	a	14.0	a	0.08	0.38	13.9	<0.19	9.7	<0.02	A0V
12	HD 283449	1.2	0.75	b	b	0.23	14.3	a	0.26	<0.09	13.7	b	0.11	0.46	14.3	0.14	10.7	<0.05	A0V
53	V1081 Tau	3.1	0.59	a,b	b	0.11	16.8	a	a	0.01	16.8	a	0.13	0.37	15.8	<0.16	10.7	<0.03	A0V
19	V892 Tau	0.5	a	...	b	0.2	14	b	b	b	c	b	b	c	0.2	b	c	b	~A0Ve
			Early-type stars from Rebull et al. (2010)																
95	HD 283751	1.5	0.39	0.49	0.26	0.82	8.0	0.13	0.23	0.36	c	0.50	0.79	0.32	c	0.31	c	0.21	B5Ve
90	HD 27923	2.3	0.24	b	0.04	0.33	12.9	a	0.18	0.07	11.8	<0.21	0.27	0.35	11.5	0.18	8.2	<0.05	B9V
91	HD 283637	1.6	0.91	b	0.1	<0.32	15.9	a	>0.04	a,b	13.7	a	0.1	0.37	13.6	0.22	c	0.1	B9.5eV
94	HD 284530	2.1	0.34	<0.01	b	0.30	13.6	a	0.30	0.09	11.7	<0.35	0.25	0.38	11.5	0.24	8.5	<0.07	B9.5V
93	2MASS0431+29	1.9	0.48	...	<0.03	a	16.6	a	a	b	17.2	a/b	<0.06	0.27	15.6	<0.24	10.9	<0.01	A1V
89	HD 27659	1.0	2.6	...	<0.19	≤0.16	10.4	a	0.4	≤0.19	10.4	<0.39	<0.23	0.47	11.6	<0.48	10.1	0.1	A3V
92	2MASS0428+27	0.3	3.5	a	<0.04	b	12	a	0.5	<0.2	12	a	<0.6	0.87	14	<0.11	9.6	0.14	A4III
			Early-type stars selected using 2MASS colors																
106	HD 26212	1.2	3.9	a	a	a	11.8	a	0.4	≤0.16	8.9	<0.33	<0.21	0.41	9.0	≤0.42	9.6	0.1	A5V
			Other																
328	HD 31305	1.8	1.7	...	b	<0.27	17.6	a	0.3	<0.09	16.3	<0.28	<0.16	0.46	15.0	<0.27	9.6	<0.02	A1V
329	AB Aur	2.4	c	...	...	...	...	...	0.2	...	...	...	...	0.40	...	...	c	c	A0Ve

Notes. B# is repeated from Table 3. S/N is the signal-to-noise ratio of the obtained spectrum.
[a] Embedded in an adjacent absorption line.
[b] Hard to distinguish from noise.
[c] Emission line present within the absorption line.

Table 5
Physical Parameters Derived through Model Atmosphere Fitting

Star	$T_{\rm eff}$ (K)	$v \cdot \sin i$ (km s^{-1})	$\log g$ (cgs)	SpT
HD 283809	21000	<50	4.0	B2V
HD 29763 = τ Tau	18000	150	4.0	B3V
HD 283751	15000	50	4.0	B5V
HD 28149 = 72 Tau	14000	75	4.0	B7V
HD 31806	14000	100	4.0	B7V
HD 28929 = HR 1445	13000	<50	4.0	B7V
HD 26571 = V1137 Tau	13000	<50	3.5	B7III
HD 284530	12000	<50	4.0	B7.5V
HD 283971	12000	50	4.0	B7.5V
HD 283304	12000	<50	3.5	B8III
HD 282276	12000	<50	3.5	B8III
HD 29647	11500	<50	3.5	B8III
HD 27923	11000	<50	4.0	B8.5V
AB Aur	11000	200	4.5	B8.5V
2MASS J04313313+2928565	11000	250	4.5	B8.5V
HD 31305	11000	150	4.5	B8.5V
HD 30378	11000	<50	4.0	B8.5V
V892 Tau	11000	100	4.5	B8.5V
HD 29935 = V1081 Tau	11000	200	4.5	B8.5V
HD 283637	11000	50	4.0	B8.5V
BD+23 607	10000	<50	4.0	A0V
HD 283449	10000	<50	4.0	A0V
HD 27659	9000	<50	3.5	A1III
2MASS J04285940+2736254	9000	<50	3.5	A4III
HD 26212	8500	<50	3.5	A5III

where χ is the fraction of the star's luminosity (L_*) above 6 eV and d is the distance from the star with the normalization constant appropriate for a B8V star.

In the cases of interest here, the brightest part of the illuminated nebula is a few arcminutes wide, which, at a fiducial distance of 140 pc, corresponds to ~0.1 pc. For comparison, using the Tielens (2005) formulation, the H II region expected for a constant density pure-hydrogen region with electron number density $n_e = 10^3$ cm^{-3} surrounding a B0V star is 0.4 pc (and would produce detectable radio emission), while for a B5V or B8V star the Strömgren radius, $\mathcal{R}_s$, is about 0.03 pc or 0.02 pc, respectively (and usually would not be detectable in the radio). Note that $\mathcal{R}_s \propto n_e$, so local overdensities can allow the PDRs to exist closer to the star thus heating them to higher temperatures. Therefore, if a dust slab were located at a few hundredths of a parsec from a B8 dwarf, the FUV radiation field it would experience is $G_0 \simeq 2$. Using $A_V \simeq 1$ for the slab, we then get $T_d \sim 10$ K. However, this oversimplified picture overlooks important processes within PDRs such as cooling through trace species such as [O I] and [C II], and the inhomogeneities in the dust cloud as indicated by the changing morphology of the nebulae toward the B stars with wavelength.

Our calculations with *DUSTY* were conducted assuming a power-law grain size distribution according to the Mathis–Rumpl–Nordsieck model (Mathis et al. 1977). As expected, when the optical depth or the physical thickness of the simulated slab is reduced, the scattered and thermal components of the output flux both decrease. If the dust temperature is lowered, then the thermal emission peak increases relative to the primary (scattered stellar flux) peak. Notably, the shape of the thermal bump flattens and broadens if the relative abundance of amorphous carbon to graphite increases, whereas increasing the relative abundance of silicates produces the broad 10 and 18 μm features.

We model the dust surrounding 72 Tau, HD 29647, HD 282276, and HD 31305 as slabs, and make an attempt to reproduce their spectral energy distributions (SEDs) using the *DUSTY* code. Our results appear in Figure 10 and are discussed for the individual stars in the next section.

3. INDIVIDUAL EARLY-TYPE OBJECTS PLAUSIBLY ASSOCIATED WITH TAURUS

In this section, we consider the collective set of plausible early-type members of Taurus based on the various lines of evidence for their physical association with the clouds.

Above, we discussed the kinematic and distance evidence for association of HD 28929 (HR 1445), HD 29763 (τ Tau), HD 26212, and HD 31305 with Taurus. Additionally, the early-type sources HD 31648, AB Aur, HD 27659, and HD 283815 have several lines of evidence that favor their association with Taurus but do not meet all of our stated criteria, mostly due to missing data.

Furthermore, within the footprint observed by *Spitzer*, six B-type stars (IC 2087-IR, 72 Tau, V892 Tau, HD 282276, HD 29647, and HR 1445) are seen in the multiband *Spitzer* images to illuminate mid-IR reflection/scattered-light nebulae, not all of which can be kinematically associated with Taurus. As mentioned above, HR 1445 was also picked out by our distance and kinematic membership selection criteria. The nebular structure is illustrated in Figures 11–16. With the exception of IC 2087, which has a bright optical nebula, optical scattered light is weak or absent among our sample. Furthermore, there is relatively little extended emission in the near-IR (J, H, K_s bands), with the wavelength of peak emission in the nebular regions typically being 8 or 24 μm. The morphologies of the nebulae are quite varied. They extend up to a few arcminutes and can appear circular or squarish, some of them being asymmetric and highly striated.

For both kinematically selected and nebular-selected objects, we constructed SEDs as shown in Figure 17. We used the following data in making the SEDs: (1) submillimeter: SCUBA/Andrews & Williams (2005); (2) IR: *Spitzer*, 2MASS, *AKARI*, *IRAS*; (3) optical/UV: NOMAD, *Galaxy Evolution Explorer* (*GALEX*). Counterparts within 1 arcsec of the source were chosen, with the exception of *IRAS* counterparts.

As reviewed by Williams & Cieza (2011), for young pre-main-sequence stars red *Spitzer*/IRAC colors indicate excess emission from circumstellar disks and envelopes, whereas excess emission at 24 μm but not in the shorter wavelength Infrared Array Camera (IRAC) bands is indicative of a disk with an inner hole. At slightly later stages, the dust is attributed to second-generation "debris" rather than primordial material. IR excess could also be attributed to dust shells around evolved stars, or illumination of nearby interstellar material, irrespective of any physical association of it with the star.

We also constructed various color–magnitude diagrams and overplotted isochrones (see Figure 18) to assist in the assessment of stellar age, assuming that the distance of Taurus is appropriate for each source. The unknown stellar multiplicity and photometric error add substantial uncertainty to the stellar age estimate. Also, because of the rapid evolution of high-mass stars, the age derived via isochrones is very sensitive to the reddening correction, which is not insignificant, and which we have derived assuming a plausibly invalid constant R_V of 3.1. All these factors together preclude accurate determination of the stellar ages of our sample, but we present the resulting color–magnitude diagram for completeness.
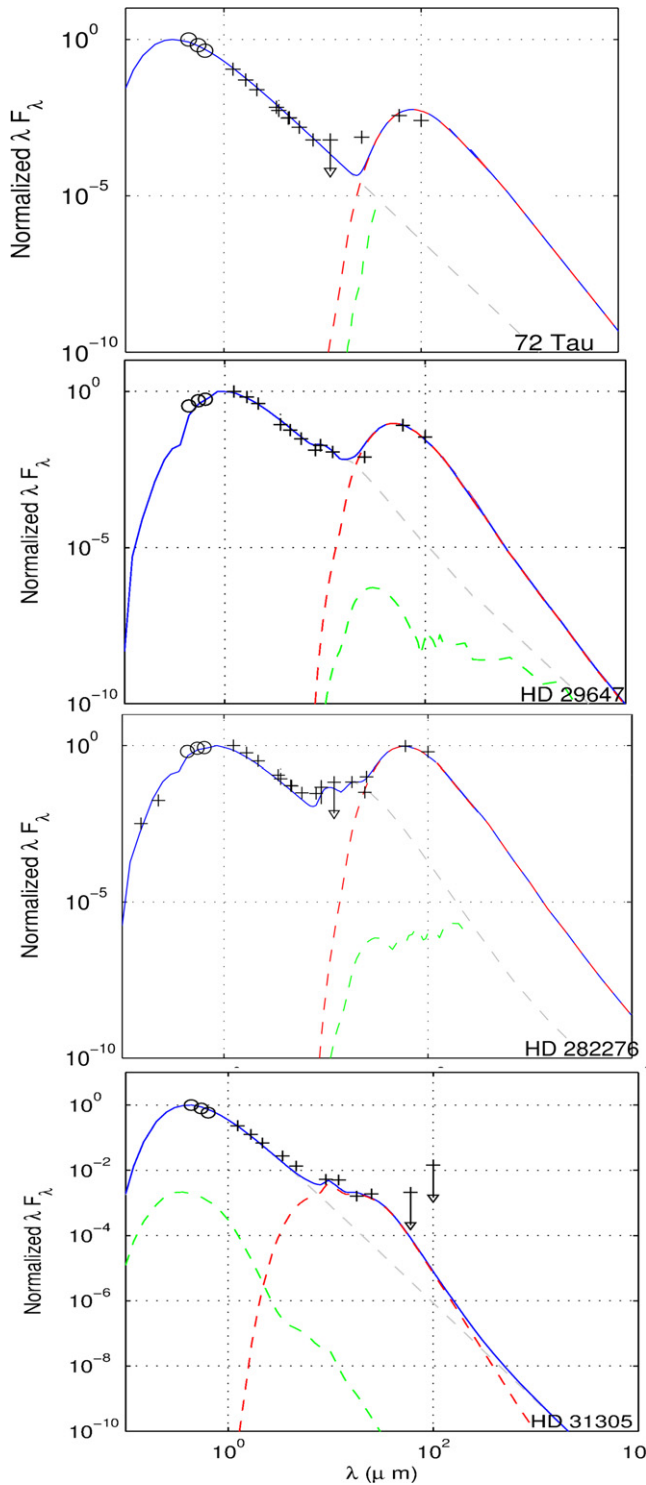
Figure 10. Modeling the SEDs (black data points) of some sources having far-infrared excess using *DUSTY*. For each of the sources, the attenuated blackbody representing the star is the gray dashed line, the contribution from the thermal and scattered emission components from the associated dust slab is shown as red and green dashed lines, respectively, and the blue solid line represents the total model output. Photometric points with error bars are shown; the circles represent *BVR* photometry that is reported without errors. *72 Tau*: a dust slab having 40 K temperature at the boundary closest to 72 Tau roughly reproduces the SED. *HD 29647 Tau*: two slab components are required to reproduce the SED, one chosen to have a dust temperature of 500 K to reproduce the $10\,\mu$m silicate feature, and another one at about 45 K. *HD 282276*: two dust slabs, having inner-edge temperatures of 200 K and 35 K are required to faithfully reproduce the SED. *HD 31305*: the inner-edge dust temperature was found to be 350 K.

(A color version of this figure is available in the online journal.)

We now discuss our findings for individual sources, beginning with those illuminating nebulae in the *Spitzer* and then moving on to other candidates that we have assessed.

3.1. IC 2087

The IC 2087 nebula (Figure 11) is brightest at optical wavelengths and is less prominent at *Spitzer* wavelengths, a unique illumination pattern among our sample. The SED (Figure 17) of the associated point source (IC 2087-IR = IRAS 04369+2539 = Kim 1-41) is consistent with an early-type Class I–Class II YSO seen through ∼15 mag of visual extinction. The foreground extinction is claimed to be $A_V < 1$ (Frerking et al. 1982), and hence the majority of the extinction toward IC 2087-IR should be due to circumstellar material (Shuping et al. 2001).

This source is a known YSO member of Taurus. High veiling has precluded accurate determination of its spectral type, but Elias (1978) classified it as B5 based on the bolometric luminosity. We were unable to derive a spectral type from either the SDSS spectrum or our own follow-up optical spectroscopy of this source. No spectroscopic parallax is possible given the vague spectral type. However, it appears that a proper-motion measurement exists for IC 2087-IR. White & Hillenbrand (2004) quoted an RV of 22 ± 8 km s^{-1} but with the large error bar, it is hard to tell whether the measurement is consistent with the RV membership criterion used herein; furthermore, the lines used may have been dominated by outflow kinematics rather than photosphere. Nonetheless, the source is currently an accepted member of Taurus, and based on multiwavelength information, we propose that an early spectral type of B5–B8 is most appropriate.

Rebull et al. (2010) confirmed that the source has a flat spectrum in the near-to-far-IR, and report $L_{\mathrm{IR}}/L_{\mathrm{total}} = 0.41$. Weak molecular outflows, the presence of Herbig–Haro knots, mid-IR absorption features, and associated reflection nebulosity provide additional evidence of the pre-main-sequence nature of this object (e.g., Furlan et al. 2008). Hillenbrand et al. (2012) provide an extensive discussion of this source.

The nebula is apparently the result of complex radiative transfer of an emitting source seen through a three-dimensional, non-uniform distribution of circumstellar dust that both obscures the central source and produces significant amounts of scattered light asymmetrically distributed with respect to the IR point source. We do not attempt to model the emission here, but see Hillenbrand et al. (2012) for an accretion disk and weak envelope fit to the SED.

3.2. 72 Tau

The nebula associated with 72 Tau (HD 28149) is brightest at about ∼60 μm. It is prominent in all *IRAS* and *Spitzer* bands and is also discernible in blue optical bands. From the image cutouts (Figure 12), it is evident that the optical depth of the associated nebula is quite different at different wavelengths in the IR. The blue optical nebula appears to have been known by Cederblad (1946), and thus this feature should be referred to as Ced 34. The striated nebular morphology is similar to that observed for the Maia nebula, illuminated by the Pleiades stars. The SED (Figure 17) of 72 Tau is consistent shortward of about $10\,\mu$m with an ideal blackbody having very low reddening, but there is a longer wavelength excess. The SED morphology is similar to that of Maia as well. Kalas et al. (2002) noted that 72 Tau is a Vega-like source associated with a gas overdensity, but no rigorous analysis was performed.
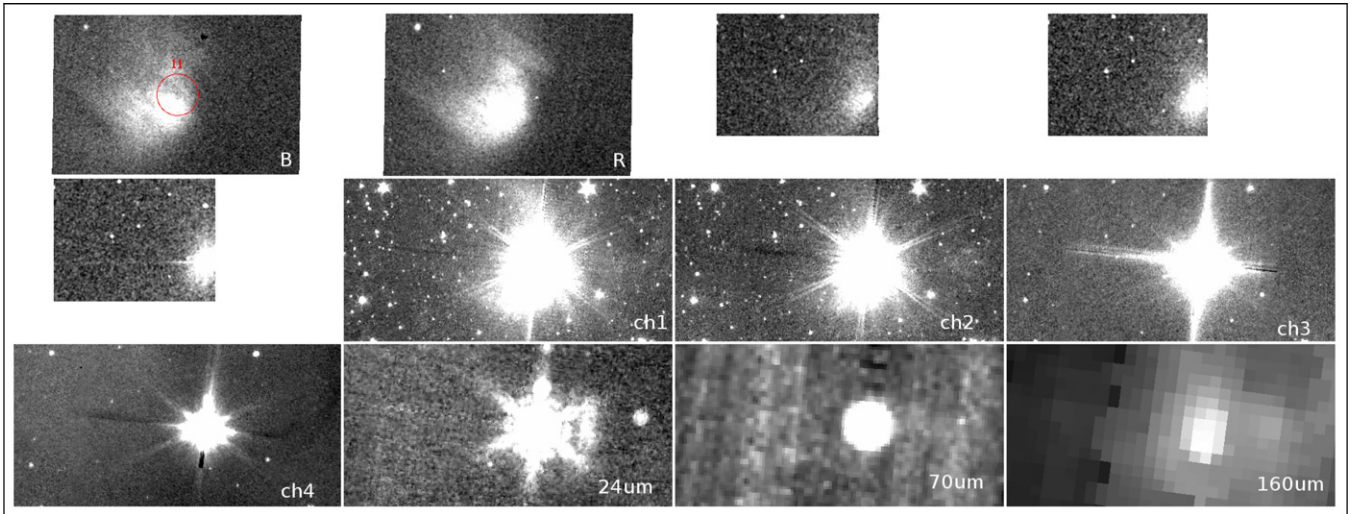
15

Figure 11. Cutouts of the IC 2087 region. Left to right: B, R images from the Palomar Observatory Sky Survey (POSS-I) and J, H images from 2MASS (Row 1), Ks band from 2MASS, and IRAC channels 3.6 μm, 4.5 μm, 5.8 μm (Row 2), IRAC 8 μm, and MIPS images 24 μm, 70 μm, and 160 μm (Row 3). The red circle in the POSS-I B-band image has a diameter of 1 arcmin for scale.

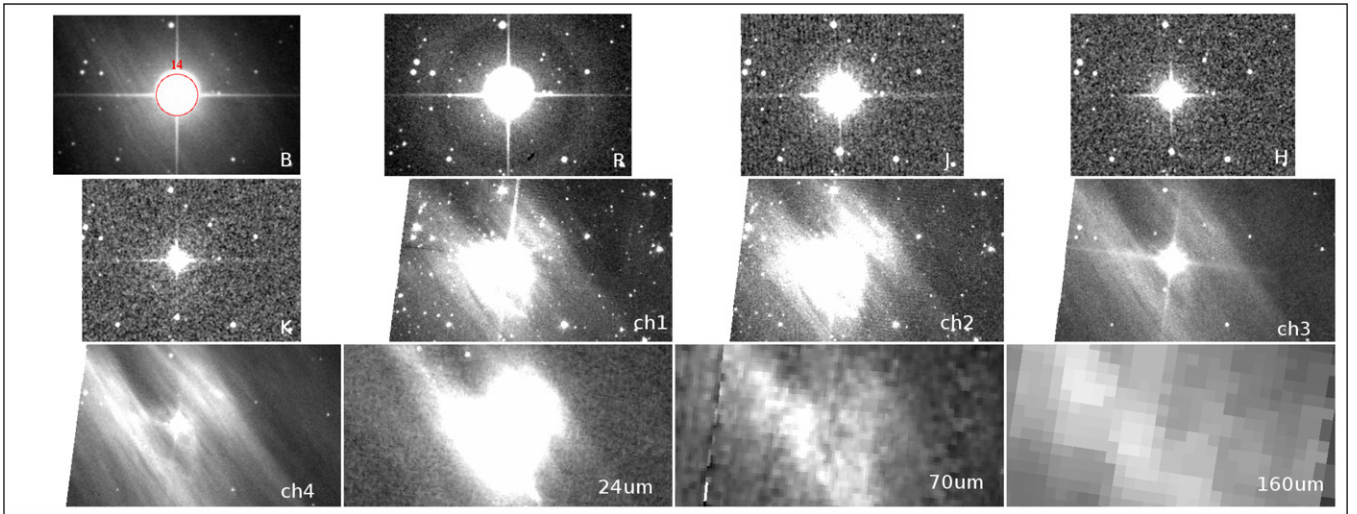(A color version of this figure is available in the online journal.)

Figure 12. Same as Figure 11 but for 72 Tau.

(A color version of this figure is available in the online journal.)
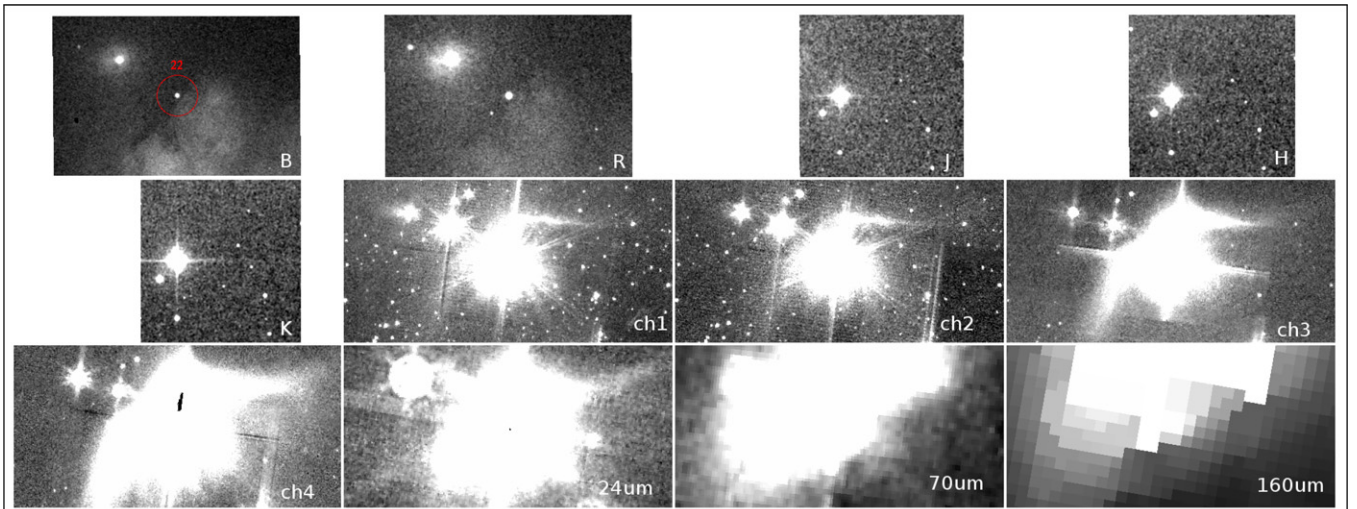
Figure 13. Same as Figure 11 but for V892 Tau/Elias 1.

(A color version of this figure is available in the online journal.)
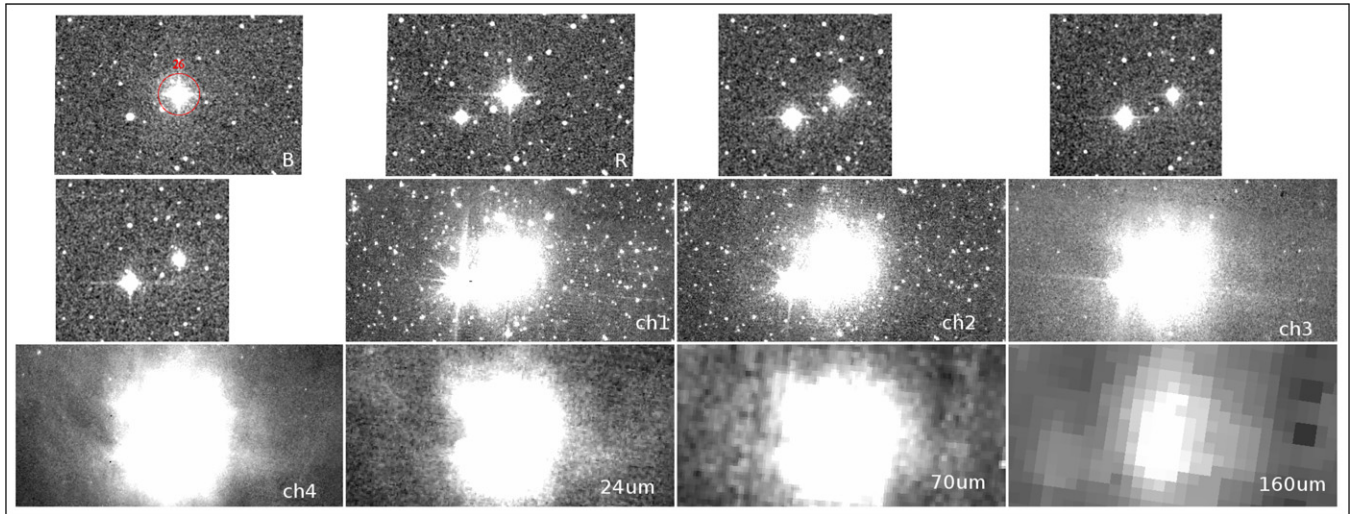
Figure 14. Same as Figure 11 but for HD 282276.
(A color version of this figure is available in the online journal.)
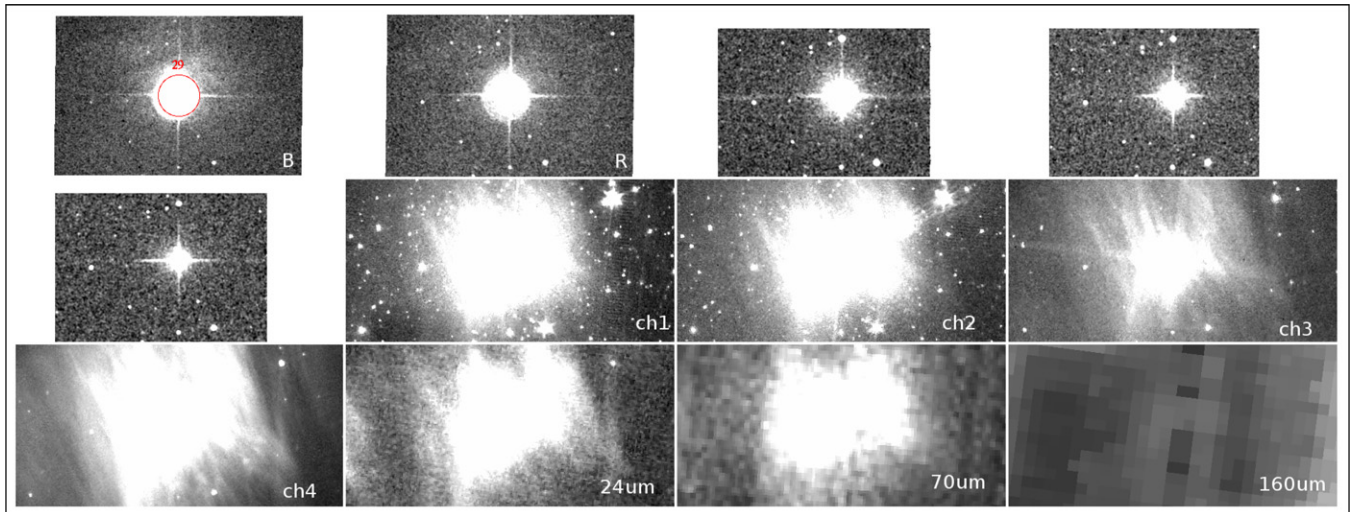
Figure 15. Same as Figure 11 but for HD 29647.
(A color version of this figure is available in the online journal.)
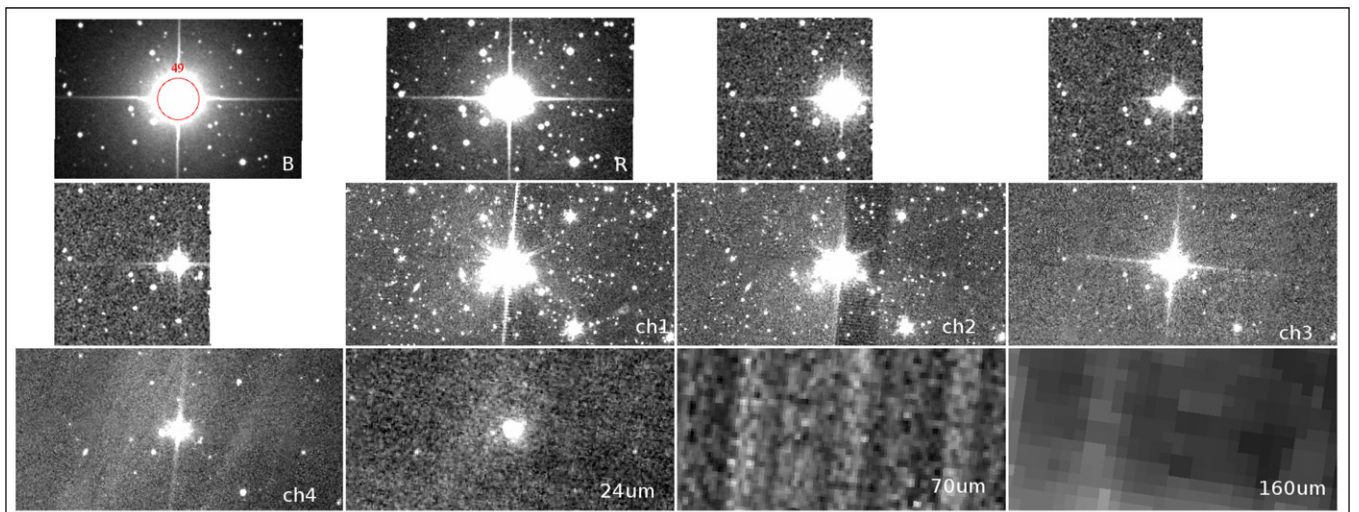
Figure 16. Same as Figure 11 but for HR 1445.
(A color version of this figure is available in the online journal.)
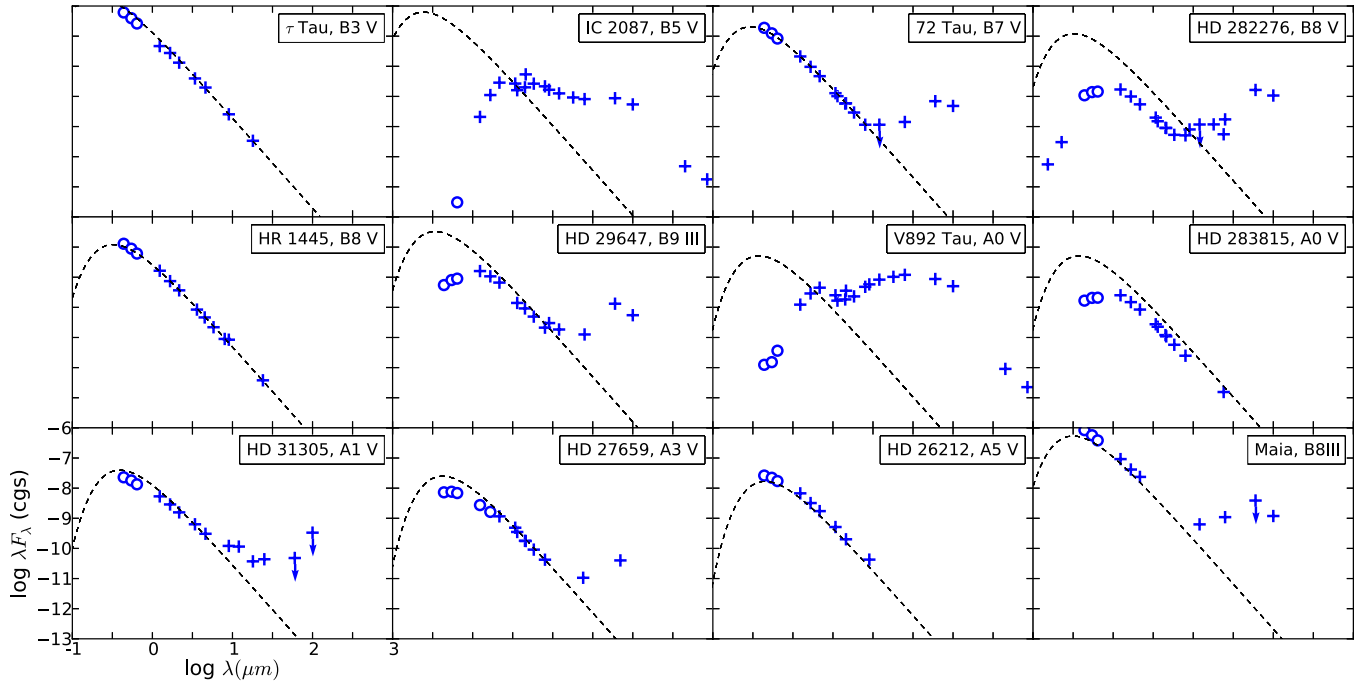
Figure 17. Spectral energy distributions (SEDs) of those sources exhibiting infrared nebulae in Figure 1 plus the candidate early-type stars we conclude are probable members of Taurus based on our assessment of distance and kinematics. Infrared excess is apparent in many objects. This may be due to the presence of a circumstellar disk associated with a pre-main-sequence stars, to a debris disk in a somewhat older main-sequence star, to a dusty atmosphere in the case of an evolved giant star, or to a chance superposition of a hot star with a nearby diffuse cloud. For comparison, an example of the chance-superposition case is also shown in the lower right panel: the Pleiades member Maia, whose SED exhibits an apparent infrared excess. The data sources include *GALEX* (ultraviolet), NOMAD (optical, *B V R*), 2MASS-PSC (near-infrared, *JHK$_s$*), *Spitzer*, *AKARI*, and *IRAS* (mid–far-infrared), and SCUBA (submillimeter). Photometric error bars are generally smaller than the symbol size; circles denote photometry lacking uncertainty (usually values from NOMAD). The dashed line in each panel represents a blackbody at 140 pc characterized by the effective temperature and radius of the star whose SED is represented in that panel. No correction for reddening has been applied though the existence of reddening can be inferred from the location of short wavelength photometry well below the nominal blackbody.

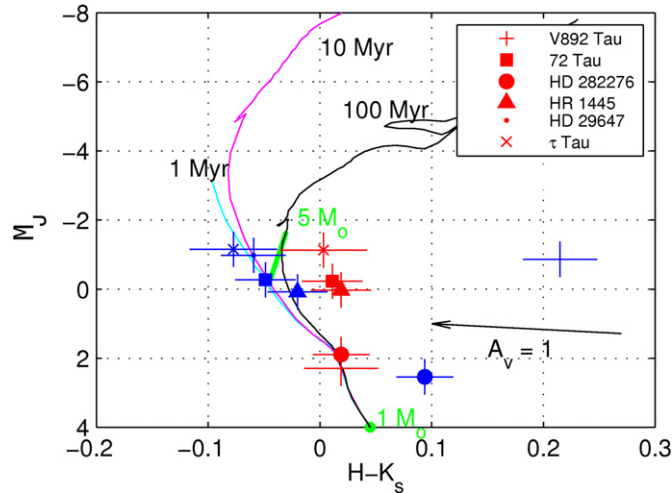(A color version of this figure is available in the online journal.)

Figure 18. Estimation of the isochronal age of some of B stars showing infrared reflection nebulae and τ Tau. Isochrones are from Girardi et al. (2002). Horizontal error bars represent the error in the 2MASS magnitudes and vertical error bars represent the uncertainty in the distance ($128 < d < 162$ pc). The blue markers are plotted using the reddening parameters from literature, while the red markers represent values derived using $R_V = 3.1$ and the Cardelli et al. (1989) reddening.

(A color version of this figure is available in the online journal.)

We arrive at a spectral classification of B7V for 72 Tau based on our follow-up spectroscopy. The *Hipparcos* distance to this star is 127 ± 12 pc while our estimate of spectroscopic parallax is 161 ± 3 pc. Walter & Boyd (1991) quoted a spectroscopic

parallax distance of 179 pc and proposed that this star is a member of Taurus and the Cas-Tau OB association. The study by de Zeeuw et al. (1999), however, does not acknowledge this star as a member of the Cas-Tau association. Kenyon et al. (1994) found a similar distance of 178 pc based on a B5V spectral type. If the *Hipparcos* distance is accurate, then 72 Tau would lie close to the nearer edge of the Taurus cloud whereas if the further distance estimates are correct the star is at the back edge of (our distance) or behind (literature distances) the cloud. Both the proper motion and the RV of this star are consistent with the Taurus group (as defined by Luhman et al. 2009). We conclude that it is very likely that 72 Tau belongs to Taurus, although in the past (Whittet et al. 2001) the star has been considered a background source in studies of the Taurus clouds.

Previous age analysis in the literature (Westin 1985) suggested an age of 20 Myr based on *ubvyβ* photometry and theoretical stellar evolution models. From our spectral analysis, 72 Tau is clearly a main-sequence star, which, after consideration of its spectral type, tells us that it is at least several Myr old and at most 170 Myr old; we are unable to place any further constraints on its age.

We were able to reproduce the SED with *DUSTY* using the parameters: (1) $T_{\rm eff} = 12,500$ K blackbody as the external radiation source; (2) dust composition with silicates from Draine & Lee (1984) and amorphous carbon from Hanner (1988) in a ratio of 1:4 (however, output not very sensitive to this ratio so long as silicate fraction is less than 1); (3) a 40 K dust temperature at the edge nearest to the external source; (4) a $0.55\,\mu$m optical depth of 0.1 (corresponding to $A_V \simeq 0.1$). The resultant ratio of the dust contribution to the observed

flux of the central star, a B7V-type blackbody, is about 1:200. This final model of the SED is shown in Figure 10. Since the fraction of the observed flux contributed by dust emission is much less compared to that contributed by the central star itself, we conclude that the nebula is not a PDR, and we do not expect any free–free emission (indicative of an ionizing front) from it.

3.3. V892 Tau

In the optical bands, V892 Tau (also known as Elias 1 or more properly Elias 3-1) appears to be a point source with an associated faint reflection nebula (Figure 13). The nebular structure is brightest at about 24 μm. Like IC 2087-IR, it is heavily reddened with a significant envelope component to its circumstellar environment. The SED (Figure 17) is that of a Class I–Class II source. Rebull et al. (2010) report it as a flat-spectrum source in the near-to-far-IR, having L_{IR}/L_{total} = 0.089. V892 Tau is a double-star system (Smith et al. 2005) with a circumbinary disk (Monnier et al. 2008).

This Herbig Ae/Be system is a well-accepted member of Taurus with reported spectral types ranging from B8 to A6. Our spectral type is B8.5V to ∼A0Ve. The optical spectrum also shows Balmer emission lines, further evidence of its youth and likely membership. Our derivation of the spectroscopic parallax distance for this star has a large uncertainty, possibly enhanced by reddening law uncertainties. The probability associated with the χ^2 analysis confirms that this source is a proper-motion member of Taurus. As for IC 2087-IR, the circumstellar environment is complex and we do not attempt to model the emission.

3.4. HD 282276

The nebula associated with HD 282276 (Figure 14) is evident only in the *Spitzer*/IRAC and MIPS bands, and not in the 2MASS or shorter wavelength bands. The nebula appears to be circular and optically thick at *Spitzer* wavelengths. This source shows considerable IR excess in its SED (Figure 17) beyond 10 μm. The two peaks in the IR excess suggest two different dust components from either two different radii or two different compositions contributing to the IR emission.

Rebull et al. (2010) have classified HD 282276 as a pending member of Taurus which needs additional follow-up; they tentatively categorized it as a Class II YSO. The spectrum of this star is B8V in our analysis but it does not show any emission lines. Both the spectroscopic parallax distance and the proper motion are inconsistent with Taurus. We estimated the reddening to be A_V = 2.8, and a spectroscopic parallax distance of 422 ± 52 pc, which means that it lies closer to the distance of Perseus than Taurus. We speculate that this star could be associated with the Perseus star-forming region, which has a mean proper motion of about μ_α = 5 mas yr^{-1}, μ_δ = −12 mas yr^{-1} (de Zeeuw et al. 1999 and PPMXL catalog), quite consistent with the measured values for HD 282276. However, the derived distance is somewhat large, even for Perseus, and the star is offset to the east of the main Perseus cloud. There is no RV measurement.

The fact that the star illuminates a reflection nebula in the IR (see Figure 1) suggests the presence of cloud material, perhaps associated with a low column density extension of the classical Perseus region. It is also possible that HD 282276 is similar to several Pleiades member stars, with the star randomly encountering a local overdensity in the ISM.

The ∼3 arcmin wide size of the nebula corresponds to a roughly 0.4 pc diameter structure at 420 pc. The H II region for

a B8V star surrounded by a pure-hydrogen nebula would be about 0.02 pc in diameter, and as the two values are inconsistent (even if our distance estimate is wrong by a factor of three), we believe that the nebula is not a PDR immediately surrounding the H II region. The SED shows two bumps in the IR, indicative of contribution from two different dust components. We can reproduce this SED with *DUSTY* using the parameters for slab A: (1) a blackbody with T_{eff} = 11,400 K as the external radiation source; (2) silicate grains from Draine & Lee (1984); (3) a 200 K dust temperature at the edge nearest to the external source; (4) a 0.55 μm optical depth of 1.4. The output of slab A summed with a 6:1 contribution from the star (blackbody) was fed into slab B, which was modeled to have the same dust composition and grain size distribution of slab A, and a dust temperature of 35 K at the edge, with visual optical depth of 1.6. Together, the optical depth adds up to 3, corresponding to $A_V \simeq$ 2.8, approximately the average extinction through the Taurus dark cloud. The dust composition is only suggestive; the bump at 10 μm is much too broad to guess the silicon abundance. However, while we note that the increase of amorphous carbon abundance relative to silicon results in a broad spectral feature at ∼0.12 μm and flattening of the thermal bump, we expect the relative amorphous carbon content to be small. Also, this broad bump makes it difficult to interpret the temperature of slab A, and we note that the edge temperature for this slab can lie anywhere between 100 and 300 K.

3.5. HD 29647

Multiwavelength images of HD 29647 (Figure 15) clearly show a striated nebulosity similar to that associated with Pleiades stars. Even the SED is similar to that of Maia, a Pleiades member; both are shown in Figure 17. The source is frequently used in interstellar column density and extinction law studies, and has a rich literature.

HD 29647 is known as a heavily reddened Hg–Mn B6-7 IV or B8 III star. From our spectrum, we classify it as a B9 III spectral type and can confirm the presence of Hg absorption. Our analysis results in a spectroscopic parallax distance of 160 ± 1 pc, consistent with Taurus membership. However, as we do not have reliable estimates for the intrinsic colors of B-type giant stars, this distance estimate might have a systematic error much greater than the quoted uncertainty. The *Hipparcos* parallax distance to HD 29647 is 177 ± 35 pc. Based on proper-motion analysis, the star is probably a non-member. There is no RV measurement; however, Adelman et al. (2001) state that the RV of the star "closely matches that of the foreground cloud" with unfortunately no quantitative detail given.

The fact that HD 29647 illuminates a bright IR nebula is, however, a compelling reason to associate this star with the far side of Taurus. Whittet et al. (2004) argue that the visual extinction of 3.6 mag for HD 29647 and 5.3 mag toward an adjacent sightline suggests that this star lies within a diffuse cloud that is slightly beyond the molecular gas constituting TMC-1. These authors also mention the existence of IR excess based on *IRAS* data as an argument for the proximity of HD 29647 to small grains associated with the cloud. A scenario in which HD 29647 was born from the Taurus cloud and ended up having different motion can be envisaged (for example, through ejection from a binary/multiple-star system). Given the relatively low space velocity as estimated from the small proper motion, however, this scenario seems unlikely. Perhaps it was born from a cloud lying between the present-day Taurus and Perseus clouds. Being a giant star, an age between 90 Myr

and 120 Myr as deduced from stellar evolution models may be appropriate for this ∼5 $M_\odot$ star. We conclude that the nebulosity in this case is a situation similar to that of Pleiades stars.

Although we have argued that this source is probably not associated with Taurus, it does illuminate nebulosity and has a substantial IR excess. We see on inspection of the SED that there is a broad silicate feature evident at 10 μm, and another thermal bump at about 60 μm. On modeling this emission with *DUSTY*, we find that two dust components are required to explain this. One produces the broad silicate feature, requiring a dust temperature at the inner boundary between 400 and 2000 K. The cooler limit comes from a fit to the thermal bump of the dust continuum emission. The hotter temperature limit is defined by the fit of the SED to optical data points. We note that as dust evaporates somewhere between 1000 K and 2000 K depending on the exact composition (e.g., Duschl et al. 1996; Speck et al. 2000), dust temperatures at the upper end of the range become unphysical. We assume somewhat arbitrarily a 500 K temperature for the first component but the use of different temperatures within the range specified above does not affect the overall fit substantially. The second dust component is characterized by a temperature of about 45 K, which is defined by the peak of the thermal bump seen at tens of microns. To reproduce the SED as shown in Figure 10, we used (1) a blackbody with $T_{\rm eff} = 10{,}900$ K as the external radiation source; (2) dust composition of silicates from Draine & Lee (1984) (with the output not very sensitive to the composition); (3) dust temperature at the edge nearest to the external source: 500 K for slab A and 46.5 K for slab B; (4) optical depth of 0.1 and 4 at 0.55 μm for slabs A and B, respectively (we need $\tau_A + \tau_B \simeq 4$, so that the total A_V for this star equals about 3.6). The output from slab A was passed as input to slab B, and thus the overall output was calculated. To the output of slab B, another contribution from the output of slab A had to be added (in a 1:10 ratio) to the result of *DUSTY* in order to reproduce the observed flux.

3.6. HR 1445

The slight nebulosity associated with HR 1445 = HD 28929 is discernible only in the 8 and 24 μm bands, with a striated morphology evident at 8 μm (Figure 16). The SED (Figure 17) does not reveal any IR excess out to 24 μm and neither the star nor any nebular emission is seen at 70 and 160 μm.

HR 1445 is known as a peculiar star, an Hg–Mn main-sequence star of spectral-type B8. Our spectral analysis also suggests a B8 (dwarf) star and we do see a weak Hg signature. The spectroscopic parallax distance is 136 ± 15 pc, and in good agreement with its *Hipparcos* parallax distance of 143 ± 17 pc. Walter & Boyd (1991) derived a spectroscopic parallax distance of 158 pc while Kenyon et al. (1994) found 137 pc. From our χ^2 probability test, we deduce secure proper-motion membership. HR 1445 also has an RV consistent with that of Taurus. The good agreement of the distance, proper motion, and RV of this star with that expected for Taurus members provides strong support to the idea of HR 1445 being a Taurus member.

The age of this star, because it is main sequence, can be constrained only to less than a few hundred Myr, within 1σ uncertainty. Westin (1985) quoted the age of this star as 60 Myr, in which case it would be an unlikely member of Taurus. HR 1445 is located toward a region of Taurus that is devoid of dense material along the line of sight. One might argue, to explain the nebulosity, that HR 1445 is located within a diffuse dust screen behind Taurus, just like HD 29647.

While HR 1445 shows hints of nebulosity, there is no IR excess and because of the wide range of unconstrained parameter space allowed in the models we do not attempt a *DUSTY* model.

3.7. τ Tau

The τ Tau = HD 29763 region was not covered by any of the *Spitzer* surveys. However, examination of *WISE* image data reveals a compact, nebulous feature at 12 and 22 μm, similar to that observed for HR 1445. Also similar to the situation for HR 1445, the SED (Figure 17) of τ Tau does not reveal any IR excess out to 22 μm and the spectrum does not show the presence of any emission lines.

This source is a well-studied binary system composed of B and early A dwarfs (e.g., Cvetkovic & Ninkovic 2010). From our B3V spectral type, we derive a spectroscopic parallax distance of 137 ± 9 pc. The *Hipparcos* parallax distance is 122 ± 13 pc. The value from Walter & Boyd (1991) is 142 pc. Both the proper motion and system RV of τ Tau are consistent with Taurus group V (as defined in Luhman et al. 2009), toward which it lies. If it is a main-sequence star, as the spectrum indicates, then we can constrain the age as being ≲40 Myr. Westin (1985) derived 20 Myr. Since the spectral type is so early, τ Tau is plausibly coeval with the low-mass T Tauri members of Taurus.

τ Tau also lies toward that region of Taurus which is devoid of dense material. A visual extinction of about 0.4 mag is derived. Only 1.6 deg away from τ Tau is HP Tau/G2 which has had its distance accurately measured via Very Long Baseline Array (VLBA) at 161 pc, whereas we find 130 pc as the distance to the binary system; this would suggest a mainly line-of-sight separation of about 30 pc between the two stars. Indeed, HP Tau/G2 has higher reddening with $A_V = 2.6$ quoted by Rebull et al. (2010). We thus conclude that the τ Tau is associated with the near side of the Taurus clouds.

As for HR 1445, given that τ Tau shows hints of nebulosity but no IR excess, we do not attempt a *DUSTY* model.

3.8. AB Aur and HD 31305

AB Aur = HD 31293 is the prototypical Herbig Ae star with an assigned a spectral type of B9–A0e, consistent with our spectrum. It is a known member of Taurus with a Class II SED. We do not produce a model for this well-studied source.

HD 31305, though not part of the area mapped under the guise of the Spitzer Taurus Legacy Survey, was covered in the "C2D" (PI: N. Evans) maps. The source is not associated with nebulosity in any mid-IR, near-IR, or optical wavelength. However, it came to our attention through its proximity to known early-type member AB Aur. In the literature, HD 31305 mainly has been used as a reference star for variability studies of AB Aur and other nearby young stars, though itself turns out to be a variable (Cody et al. 2013).

We derive a spectral type of A1V with very little reddening ($A_V \simeq 0.1$) for HD 31305, and a spectroscopic parallax distance of 174 ± 11 pc. Although this star lies at 1σ, just outside the formal distance range that we consider for Taurus membership (up to 162 pc), the star is seemingly a good candidate for membership. A secure proper-motion membership probability is found, but no RV measurements exist. Keeping these points in mind, we conclude that HD 31305 is likely a newly appreciated member of Taurus.

There is no nebulosity apparent but the SED shows IR excess in the near-to-far-IR. Investigation of its SED relative to a range of *DUSTY* models tells us that the 10 μm silicate feature is

probably strong above the blackbody line, with the second thermal bump at a longer wavelengths broad and flat. This SED morphology indicates a similar abundance of silicon and amorphous carbon. The silicate feature remains significant if the edge temperature of the dust slab is set to lie between 100 and 500 K, but this is also dependent on the optical depth. We model this SED using the following parameters for a single slab: (1) blackbody with $T_{eff} = 9400$ K ($=$A1V) as the external radiation source, (2) silicate and graphite grains from Draine & Lee (1984) in a 10:1 ratio, (3) a 350 K dust temperature at the edge nearest to the external source, (4) 0.55 μm optical depth of 0.05. The contribution of the central star relative to the thermal and scattered dust emission is 4:1. The dust emission could equivalently be modeled using a two-slab model to get a better fit, but this is not justified by the low extinction and the appearance of the nebula on 2MASS image cutouts.

3.9. HD 26212

HD 26212 also lies outside the region of the Spitzer Taurus Legacy Survey, but was not covered in C2D. Inspection of DSS, 2MASS, *WISE*, and *IRAS* images does not reveal any nebulosity toward this star. It does not have any IR excess out to 24 μm as evidenced by its SED (Figure 17).

We arrived at a spectral classification of A5V for HD 26212. The corresponding spectroscopic parallax is 115 ± 4 pc which is in agreement (within the 2σ error) with both its larger *Hipparcos* parallax as well as the new *Hipparcos* reduction (van Leeuwen 2007), $d_{HIP} = 100^{+7.8}_{-6.7}$. The proper motion of this star is consistent with Taurus, which means that it is tangentially comoving with the members of this cloud. The mean RV quoted in the literature is about 20 km s^{-1}, and within 1σ, agrees with that observed for Taurus members. The derived spectroscopic parallax yielded a visual reddening of $A_V = 0.16$. The low reddening and near distance suggests that HD 26212 lies in the outskirts of the L1498 region in Taurus. Since its spectrum suggests a main-sequence star and the spectral type is late, we cannot meaningfully constrain the age.

HD 26212 shows neither significant IR excess nor scattered light, and therefore cannot be modeled with *DUSTY*.

3.10. HD 27659, HD 283815

Both of these stars are listed as having spectral-type A0 and as probable members of Taurus based on IR excess by Rebull et al. (2010).

The multiwavelength image cutouts of HD 27659 show extended emission at 8 μm. The object is seen to be fuzzy but somewhat compact beyond this wavelength, a feature which is similar to multiwavelength image morphology of HR 1445 and τ Tau. HD 27659 also shows considerable IR excess beyond 25 μm (Figure 17). Rebull et al. (2010) find a Class II SED with $L_{IR}/L_{total} = 6 \times 10^{-4}$. Kenyon et al. (1994) classified HD 27659 as an A4V star and derived a spectroscopic parallax distance of $d = 146$ pc. Belikov et al. (2002) list HD 27659 as a member of the Perseus OB2 star-forming complex, but its proper motion renders this improbable.

For HD 283815, there is no associated IR nebulosity but Rebull et al. (2010) found the 8 μm to 24 μm flux ratio to indicate a Class III SED exhibiting a weak IR excess, though this is not readily apparent from examination of the SED (Figure 17). There is sparse literature for HD 283815.

In terms of spectroscopic parallax, HD 27659 has an implied distance based on our derivation of an A3 spectral type of 164 pc which matches our criteria of membership with Taurus.

For HD 283815 we did not obtain a spectrum, but using the literature spectral type of A0 shows that it does not meet our distance criteria, as can be discerned from the underluminous SED of Figure 17 when a 140 pc distance is assumed. In proper motion, however, the inverse is true with HD 27659 showing proper motion inconsistent with Taurus, but HD 283815 a high probability proper-motion member. RV measurements exist for neither star.

Given the evidence, at present no strong statements can be made about the membership of either star. They could be early-type members with peculiar motions, or background stars reddened due to the Taurus cloud. In both cases, there is some evidence for associated dust. HD 27659 has just two SED points within the region showing IR excess, and we hesitate to attempt fitting of a unique model to it. HD 283815 shows neither significant IR excess nor scattered light, and therefore cannot be modeled.

Of possible relevance is that lying only a quarter of a degree away from HD 27659 is HDE 283572, a Taurus member whose distance has been measured precisely by VLBA techniques. The implied distance between the two stars would be about 35 pc. From Figure 4, the proximity with a high surface density part of the cloud is evident and there is significant reddening implied for the further star HD 27659.

4. SUMMARY AND CONCLUSION

Early-type stars illuminating IR nebulae found in *Spitzer* IRAC/MIPS maps of the Taurus–Auriga molecular cloud complex led us to carry out a more comprehensive search for early-type stars in this star-forming region. We compiled a list of 329 candidate early-type stars (see Table 3) toward Taurus from (1) previously known O, B stars listed by SIMBAD; (2) proposed B stars from Rebull et al. selected to have IR excess and followed up spectroscopically; (3) stars from the 2MASS-PSC selected on the basis of photometric color; and (4) early-type stars spectroscopically identified in the SDSS. This set of stars was then tested against various membership criteria including distance, kinematics, and age criteria.

First, we provided accurate spectral-type information for about 20 stars which were spectroscopically followed up from our initial sample at the 200 inch Hale telescope at the Palomar Observatory. This, along with the magnitudes available in the literature, has helped in deriving spectroscopic parallax distances to the stars, accounting for extinction. Notably, the presence of several diffuse interstellar bands is well correlated with the estimated distances; none of the stars we believe associated based on distance or kinematic arguments with the Taurus star-forming region exhibit these features, which are seen in only more distant stars. Several of the spectra show emission lines which in two cases are associated with known YSOs and in the other two cases appear associated with background Be stars also exhibiting IR excesses.

Hipparcos parallaxes and spectroscopic parallaxes were used to select stars between 128 and 162 pc, allowing for error. Proper-motion membership was tested by calculating the χ^2 probability using the proper motion of various comoving groups in Taurus (defined by Luhman et al. 2009). RV, wherever available, has been compared with that of the previously known members of Taurus. We have also especially considered all early-type sources illuminating nebulae, regardless of whether they meet the distance and kinematic criteria.

Our final assessment of membership is shown in Table 6. Through this work, we have found three stars of

Table 6
Final List of Early-type Stars Showing Indications of Membership with Taurus

B#	HD Number	Alt. Identifier	α_{J2000} (h,m,s)	δ_{J2000} ($^\circ,',''$)	SpT	d_{HIP} (pc)	d_{SPEC} (pc)	$P(\chi^2)$ (%)	RV (km s^{-1})	Comments
					Probable members based on our analysis of distance and/or kinematics					
51	HD 29763	τ Tau	04 42 14.70	22 57 24.9	B3V	123^{+13}_{-11}	137 ± 9	5.1	12.3 ± 4.1	
25	HD 28149	72 Tau	04 27 17.45	22 59 46.8	B7V	127^{+13}_{-11}	161 ± 3	2.4	7.3 ± 2.6	IR nebula; cool dust SED
36	HD 28929	HR 1445	04 34 37.99	28 57 40.1	B8V	143^{+20}_{-16}	157 ± 3	11.5	12.6 ± 2.2	Weak nebula
19	$\cdots$	V892 Tau	04 18 40.62	28 19 15.5	$\sim$B8.5–A0Ve	$\cdots$	$\dagger$	25.7		IR nebula; Class I SED
329	HD 31293	AB Aur	04 55 45.85	30 33 04.3	A0Ve	139^{+22}_{-16}	120 ± 50	36.1	8.9 ± 0.9	Class II SED
328	HD 31305	IRAS 04526+3015	04 55 48.23	30 20 16.5	A1V	$\cdots$	174 ± 11	21.5		Cool dust SED
193	HD 31648	MWC 480	04 58 46.27	29 50 37.0	A3Ve	137^{+31}_{-21}	186 ± 48	18.8		Class II SED
106	HD 26212	$\cdots$	04 09 43.68	24 04 22.6	A5V	123^{+17}_{-14}		3.3	20.3 ± 3.9	
					Candidates with several membership indicators but that are not secure distance and kinematic members					
46	$\cdots$	IC 2087-IR	04 39 55.75	25 45 02.0	B5–B8	$\cdots$		46.7		IR and visible nebula; Class I SED; member
96	HD 283815	$\cdots$	04 42 41.18	24 41 17.9	A0	$\cdots$	268 ± 40	12.8		Meets proper motion but not distance criteria
89	HD 27659	$\cdots$	04 22 54.66	28 23 55.0	A3V	$\cdots$	164 ± 10	<0.1		Meets distance but not proper-motion criteria; cool dust SED
					Stars illuminating infrared nebulae but that cannot be associated with Taurus based on distance and kinematic criteria					
33	HD 282276	$\cdots$	04 33 04.23	29 21 49.9	B8V	$\cdots$	422 ± 52	<0.1		IR nebula; cool dust SED
48	HD 29647	IRAS 04380+2553	04 41 08.05	25 59 34.0	B9III	177^{+43}_{-29}	160 ± 1	<0.1		IR nebula; cool dust SED

Notes. (1) B# is repeated from Table 3. (2) SpT is the spectral type as revised in this work or from literature. (3) As noted elsewhere, error on d_{SPEC} corresponds to variance among calculations and underestimates the true error. (4) The probability of proper-motion membership, $P(\chi^2)$, is as discussed in Section 2.3.2. (5) The membership criteria used in this work are: $P(\chi^2) > 1\%$; $128 < d < 162$ pc within 1σ error; and $9.8 \leqslant$ RV $\leqslant 17.5$ km s^{-1} wherever radial velocity is available. (6) For the † source V892 Tau, $d_{SPEC} = 1697 \pm 1548$ pc, but $d_B = 4720$ pc while $d_K = 135$ pc.

spectral-type B, and two of spectral-type A to be newly appreciated members of Taurus. Specifically, HR 1445 (HD 28929), τ Tau (HD 29763), 72 Tau (HD 28149), HD 31305, and HD 26212 meet the kinematic and distance criteria while HD 27659 and HD 283815 show ambiguous kinematic and/or distance properties that make their membership plausible but not secure. Additional or improved space velocity information for these and several other stars could confirm their membership. These sources should be considered along with the currently accepted early-type members: IC2087-IR (B5-like luminosity but heavily self-embedded source with a continuum-emission optical and IR spectrum), the binary system V892 Tau (Elias 1; a B8–A6 self-embedded Herbig Ae/Be star with a near-equal brightness companion), the triple system HD 28867 (B8 + 2 × B9.5), AB Aur (A0e, a Herbig Ae/Be star), and HD 31648 (MWC 480; A2e, another Herbig Ae/Be star). While HD 28867 is located to the south of the main Taurus–Auriga clouds and therefore is not recovered in our search, the other known early-type members were recovered, although to varying degrees of security. Notably, more than half—but not all—of the stars listed above distinguish themselves through illumination of optical or IR nebulae. Furthermore, two-thirds—but not all—of the stars have mid-IR excesses which may be due to an extended nebula or to a more compact protoplanetary or later stage debris disk.

Among the stars with IR reflection/scattered-light nebulae, two sources (HD 28149 = 72 Tau and HD 29647) have been used as intrinsically bright background "candles" in studies of the molecular cloud's physical and chemical properties. In the case of 72 Tau, the kinematics and distance are both consistent with those of previously known members of Taurus. While chance superposition with the Taurus cloud is possible, this main-sequence star was probably born near its present environment and is truly associated with the cloud. Our assessment of HD 29647 suggests an object at similar distance to though just behind the Taurus cloud (the same conclusion was reached by Whittet et al. 2004) and with different kinematics. Both HD 29647 and 72 Tau have nebulae which appear to be morphologically similar to the striated nebulosity toward the Pleiades stars Merope and Maia. The difference is that the Taurus nebulae under study here are much fainter and much less distinct at visible wavelengths than the Pleiades cases, probably due to the amount of foreground extinction or to the spectrum of incident radiation (and less likely due to the dust properties).

Another bright nebulous source, HD 282276 (northernmost circle in Figure 1) is likely a B-type star lying background to Taurus and close to the distance of the Perseus star-forming region, although well east of it. The molecular material may also be at that further distance.

We modeled the nebular dust emission of a subset of interesting stars also showing IR excess. The dust temperatures found via this study, which account for the thermal dust emission peaks in the SEDs, are usually about 45 K. In some cases (viz., HD 282276 and HD 29647), there is evidence of two dust components contributing to the IR emission, where the higher-temperature component is between 100 K and 500 K. The distance between the nebulae and the early-type stars can be estimated by balancing the heating and cooling rates. However, the unknown composition, complicated morphology, and the self-similar nature of the radiation transfer makes the problem very challenging. Nevertheless, the IR excess tells us that the star is sufficiently close to the nebula to heat it. Kinematic information of the stars supplements this proximity information to help distinguish between association with the cloud and chance superposition.

We call attention to the fact that we have doubled the number of stars with spectral-type A5 or earlier that can be associated with the Taurus molecular cloud. This includes the earliest-type star claimed yet as a member of Taurus: the B3V star τ Tau. Nevertheless, the cloud still seems to be a factor of two short in early-type members, considering a standard log-normal form for the IMF and given its low mass and brown dwarf population that numbers at least 350.

REFERENCES

Abazajian, K. N., Adelman-McCarthy, J. K., Agüeros, M. A., et al. 2009, ApJS, 182, 543
Abt, H. A., Levato, H., & Grosso, M. 2002, ApJ, 573, 359
Adelman, S. J., Snow, T. P., Wood, E. L., et al. 2001, MNRAS, 328, 1144
Andrews, S. M., & Williams, J. P. 2005, ApJ, 631, 1134
Bally, J., Walawender, J., & Reipurth, B. 2012, AJ, 144, 143
Belikov, A. N., Kharchenko, N. V., Piskunov, A. E., Schilbach, E., & Scholz, R.-D. 2002, A&A, 387, 117
Bessell, M. S., Castelli, F., & Plez, B. 1998, A&A, 333, 231
Blaauw, A. 1956, ApJ, 123, 408
Cardelli, J. A., Clayton, G. C., & Mathis, J. S. 1989, ApJ, 345, 245
Carpenter, J. M. 2001, AJ, 121, 2851
Carroll, B. W., & Ostlie, D. A. (ed.) 2006, in An Introduction to Modern Astrophysics (2nd ed.; San Francisco, CA: Pearson)
Cederblad, S. 1946, MeLu2, 119, 1
Cody, A. M., Tayar, J., Hillenbrand, L. A., Matthews, J., & Kallinger, T. 2013, AJ, 145, 79
Cvetkovic, Z., & Ninkovic, S. 2010, SerAJ, 180, 71
de Zeeuw, P. T., Hoogerwerf, R., de Bruijne, J. H. J., Brown, A. G. A., & Blaauw, A. 1999, AJ, 117, 354
Didelon, P. 1982, A&AS, 50, 199
Dobashi, K., Uehara, H., Kandori, R., et al. 2005, PASJ, 57, 1
Draine, B. T., & Lee, H. M. 1984, ApJ, 285, 89
Ducourant, C., Teixeira, R., Périé, J. P., et al. 2005, A&A, 438, 769
Duschl, W. J., Gail, H.-P., & Tscharnuter, W. M. 1996, A&A, 312, 624
Elias, J. H. 1978, ApJ, 224, 857
Finkbeiner, D. P., Padmanabhan, N., & Schlegel, D. J. o. 2004, AJ, 128, 2577
Fitzgerald, M. P. 1970, A&A, 4, 234
Frerking, M. A., Langer, W. D., & Wilson, R. W. 1982, ApJ, 262, 590
Furlan, E., McClure, M., Calvet, N., et al. 2008, ApJS, 176, 184
Girardi, L., Bertelli, G., Bressan, A., et al. 2002, A&A, 391, 195
Goldsmith, P. F., Heyer, M., Narayanan, G., et al. 2008, ApJ, 680, 428
Gontcharov, G. A. 2006, AstL, 32, 759
Güdel, M., Padgett, D. L., & Dougados, C. 2007, in Protostars and Planets V, ed. B. Reipurth, D. Jewitt, & K. Keil (Tucson, AZ: Univ. Arizona Press), 329
Hanner, M. 1988, Grain Optical Properties, Technical Report
Hartmann, L., Stauffer, J. R., Kenyon, S. J., & Jones, B. F. 1991, AJ, 101, 1050
Herbig, G. H. 1960, ApJS, 4, 337
Hillenbrand, L. A., Knapp, G. R., Padgett, D. L., Rebull, L. M., & McGehee, P. M. 2012, AJ, 143, 37
Ivezic, Z., & Elitzur, M. 1997, MNRAS, 287, 799
Johnson, H. L. 1966, ARA&A, 4, 193
Jones, B. F., & Herbig, G. H. 1979, AJ, 84, 1872
Kalas, P., Graham, J. R., Beckwith, S. V. W., Jewitt, D. C., & Lloyd, J. P. 2002, ApJ, 567, 999

Kenyon, S. J., Dobrzycka, D., & Hartmann, L. 1994, AJ, 108, 1872
Kenyon, S. J., Gómez, M., & Whitney, B. A. 2008, in Handbook of Star Forming Regions, Vol. I, ed. B. Reipurth (San Francisco, CA: ASP), 405
Kharchenko, N. V., & Roeser, S. 2009, yCat, 1280, 0
Kharchenko, N. V., Scholz, R., Piskunov, A. E., Röser, S., & Schilbach, E. 2007, AN, 328, 889
Kirk, H., & Myers, P. C. 2011, ApJ, 727, 64
Knapp, G. R., Finkbeiner, D. P., Padmanabhan, N., & Schegel, D. J. 2007, BAAS, 38, 781
Koornneef, J. 1983, A&A, 128, 84
Kraus, A. L., & Hillenbrand, L. A. 2007, AJ, 134, 2340
Kraus, A. L., Ireland, M. J., Martinache, F., & Hillenbrand, L. A. 2011, ApJ, 731, 8
Lesh, J. R. 1968, ApJS, 17, 371
Loinard, L., Torres, R. M., Mioduszewski, A. J., et al. 2007, ApJ, 671, 546
Lombardi, M., Lada, C. J., & Alves, J. 2010, A&A, 512, A67
Luhman, K. L., Allen, P. R., Espaillat, C., Hartmann, L., & Calvet, N. 2010, ApJS, 186, 111
Luhman, K. L., Mamajek, E. E., Allen, P. R., & Cruz, K. L. 2009, ApJ, 703, 399
Maheswar, G., Lee, C. W., Bhatt, H. C., Mallik, S. V., & Dib, S. 2010, A&A, 509, A44
Mathis, J. S., Rumpl, W., & Nordsieck, K. H. 1977, ApJ, 217, 425
Miller, G. E., & Scalo, J. M. 1979, ApJS, 41, 513
Monnier, J. D., Tannirkulam, A., Tuthill, P. G., et al. 2008, ApJL, 681, L97
Morgan, W. W., Keenan, P. C., & Kellman, E. (ed.) 1943, in An Atlas of Stellar Spectra, with an Outline of Spectral Classification (Chicago, IL: Univ. Chicago Press)
Munari, U., Sordo, R., Castelli, F., & Zwitter, T. 2005, A&A, 442, 1127
Narayanan, G., Heyer, M. H., Brunt, C., et al. 2008, ApJS, 177, 341
Narayanan, G., Snell, R., & Bemis, A. 2012, MNRAS, 425, 2641
Palmeirim, P., André, P., Kirk, J., et al. 2013, A&A, 550, A38
Parker, R. J., Bouvier, J., Goodwin, S. P., et al. 2011, MNRAS, 412, 2489
Perryman, M. A. C., & ESA (ed.) 1997, The HIPPARCOS and TYCHO Catalogues. Astrometric and Photometric Star Catalogues Derived from the ESA HIPPARCOS Space Astrometry Mission (ESA Special Publication, Vol. 1200; Noordwijk: ESA)

Pickles, A. J. 1998, PASP, 110, 863
Rebull, L. M., Koenig, X. P., Padgett, D. L., et al. 2011, ApJS, 196, 4
Rebull, L. M., Padgett, D. L., McCabe, C., et al. 2010, ApJS, 186, 259
Rieke, G. H., & Lebofsky, M. J. 1985, ApJ, 288, 618
Roeser, S., Demleitner, M., & Schilbach, E. 2010, AJ, 139, 2440
Schmidt-Kaler, T. 1982, in The Physical Parameters of the Star, ed. K. Schaifers & H. H. Voigt (Berlin: Springer), 18
Shuping, R. Y., Chiar, J. E., Snow, T. P., & Kerr, T. 2001, ApJL, 547, L161
Skrutskie, M. F., Cutri, R. M., Stiening, R., et al. 2006, AJ, 131, 1163
Smith, K. W., Balega, Y. Y., Duschl, W. J., et al. 2005, A&A, 431, 307
Speck, A. K., Barlow, M. J., Sylvester, R. J., & Hofmeister, A. M. 2000, A&AS, 146, 437
Takita, S., Kataza, H., Kitamura, Y., et al. 2010, A&A, 519, A83
Tielens, A. G. G. M. (ed.) 2005, The Physics and Chemistry of the Interstellar Medium (Cambridge: Cambridge Univ. Press)
Torres, R. M., Loinard, L., Mioduszewski, A. J., & Rodríguez, L. F. 2007, ApJ, 671, 1813
Torres, R. M., Loinard, L., Mioduszewski, A. J., & Rodríguez, L. F. 2009, ApJ, 698, 242
Torres, R. M., Loinard, L., Mioduszewski, A. J., et al. 2012, ApJ, 747, 18
Ungerechts, H., & Thaddeus, P. 1987, ApJS, 63, 645
van Leeuwen, F. 2007, A&A, 474, 653
Walter, F. M., Beck, T. L., Morse, J. A., & Wolk, S. J. 2003, AJ, 125, 2123
Walter, F. M., & Boyd, W. T. 1991, ApJ, 370, 318
Walter, F. M., Brown, A., Mathieu, R. D., Myers, P. C., & Vrba, F. J. 1988, AJ, 96, 297
Westin, T. N. G. 1985, A&AS, 60, 99
White, R. J., & Hillenbrand, L. A. 2004, ApJ, 616, 998
Whittet, D. C. B., Gerakines, P. A., Hough, J. H., & Shenoy, S. S. 2001, ApJ, 547, 872
Whittet, D. C. B., Shenoy, S. S., Clayton, G. C., & Gordon, K. D. 2004, ApJ, 602, 291
Williams, J. P., & Cieza, L. A. 2011, ARA&A, 49, 67
Wolff, S. C., & Preston, G. W. 1978, ApJS, 37, 371
Zacharias, N., Monet, D. G., Levine, S. E., et al. 2005, yCat, 1297, 0